Active suppression of Ostwald ripening: Beyond mean-field theory

Paul C. Bressloff [ORCID]

Department of Mathematics, University of Utah, Salt Lake City, Utah 84112, USA

Active processes play a major role in the formation of membraneless cellular structures (biological condensates). Classical coarsening theory predicts that only a single droplet remains following Ostwald ripening. However, in both the cell nucleus and cytoplasm there coexist several membraneless organelles of the same basic composition, suggesting that there is some mechanism for suppressing Ostwald ripening. One potential candidate is the active regulation of liquid-liquid phase separation by enzymatic reactions that switch proteins between different conformational states (e.g., different levels of phosphorylation). Recent theoretical studies have used mean-field methods to analyze the suppression of Ostwald ripening in three-dimensional (3D) systems consisting of a solute that switches between two different conformational states, an S state that does not phase separate and a P state that does. However, mean-field theory breaks down in the case of 2D systems, since the concentration around a droplet varies as $\ln R$ rather than R^{-1}, where R is the distance from the center of the droplet. It also fails to capture finite-size effects. In this paper we show how to go beyond mean-field theory by using the theory of diffusion in domains with small holes or exclusions (strongly localized perturbations). In particular, we use asymptotic methods to study the suppression of Ostwald ripening in a 2D or 3D solution undergoing active liquid-liquid phase separation. We proceed by partitioning the region outside the droplets into a set of inner regions around each droplet together with an outer region where mean-field interactions occur. Asymptotically matching the inner and outer solutions, we derive leading-order conditions for the existence and stability of a multidroplet steady state. We also show how finite-size effects can be incorporated into the theory by including higher-order terms in the asymptotic expansion, which depend on the positions of the droplets and the boundary of the 2D or 3D domain. The theoretical framework developed in this paper provides a general method for analyzing active phase separation for dilute droplets in bounded domains such as those found in living cells.

I. INTRODUCTION

Membraneless subcellular structures (biological condensates) are ubiquitous in both the cytoplasm and nucleus of cells. Examples include stress granules and processing (P) bodies in the cytoplasm [1], and nucleoli and Cajal bodies in the nucleus [2]. All of these structures consist of enhanced concentrations of various proteins and RNA, and proteins are continually exchanged with the surrounding medium. Major insights into the nature of biological condensates have been obtained from studies of P granules in germ cells of *Caenorhabditis elegans*. P granules are RNA and protein-rich bodies located in the cytosplamic region around the nucleus (perinuclear region), which play a role in asymmetric cell division. Their relatively large size (diameters of 2–4 μm) make them particularly amenable to quantitative analysis [3]. In particular, it has been shown that P granules fuse with one another and subsequently relax back into a spherical shape, flow freely under shear forces, and deform around surfaces of other structures. Moreover, photobleaching experiments have demonstrated that proteins are highly mobile within P granules and exchange rapidly with the surrounding cytoplasm. Taken together with subsequent studies of many other condensates, there is a growing body of evidence supporting the hypothesis that membrane-less organelles are multicomponent, viscous liquidlike structures that form via liquid-liquid phase

separation (see the reviews [4–8] and references therein). The onset of phase separation can be regulated by a number of factors: changes in protein or RNA concentration via gene expression, post-translational modifications in protein structure, and changes to salt or proton concentration and/or temperature (osmotic or pH shocks) [3]. Although intracellular biological condensates are multicomponent structures, typically containing dozens of different types of proteins and RNA, it is possible to reconstitute *in vitro* droplets that have similar features using only one or two molecular components [9,10]. This suggests that, at least in some cases, a single protein may be necessary and sufficient to drive assembly.

Classical liquid-liquid phase separation occurs when it is thermodynamically favorable for a homogeneous solution to separate or demix into two coexisting liquid phases with different densities, a high-density phase ϕ_b and a low-density phase ϕ_a. From a kinetic perspective, there are two basic dynamical mechanisms for phase separation, depending on which region of the associated phase diagram the homogeneous solution is initially placed by, for example, changing the temperature: (i) spinodal decomposition, which occurs when the solution is in a thermodynamically unstable state, and (ii) nucleation and growth, which occurs when the solution is in a metastable state. Spinodal decomposition involves the rapid demixing from one thermodynamic phase to two

coexisting phases due to the fact that there is essentially no thermodynamic barrier to nucleation of the two phases. In early stages of phase separation, solute molecules cluster together to form microscopic solute-rich domains dispersed throughout the liquid. These droplets then rapidly grow and coalesce to form macroscopic clusters or droplets. As phase separation proceeds, the growth of clusters approximately ceases when the local concentration reaches ϕ_a or ϕ_b, resulting in the separation of the solution into domains of low- and high-solute concentrations. Although the concentration no longer changes within each droplet, the size and shape of the droplets evolve due to the effects of interfacial tension τ_s. If the characteristic size of a droplet is R, then the interfacial energy per unit volume is τ_s/R. Structural changes of the droplets can thus reduce this contribution to the free energy by effectively increasing the average size R, in a coarsening process known as Ostwald ripening [11,12]. Diffusion also plays a role in coarsening because the concentrations ϕ_a and ϕ_b in a neighborhood of a droplet deviate slightly from their thermodynamic values according to the Gibbs-Thompson law [13]. The first quantitative formulation of Ostwald ripening was developed by Lifshitz and Slyozov [11] and Wagner [12], and is commonly referred to as classical LSW theory. These authors derived an equation for the number density of droplets in the dilute regime (total volume fraction of droplets is small), under the crucial assumption that the interaction between droplets can be expressed solely through a common mean field.

A major feature of biological cells is that they are often driven away from equilibrium by multiple energy-consuming processes, including adenosine triphosphate–(ATP) driven protein phosphorylation. There is growing experimental evidence that active processes also influence the phase separation of biological condensates [7,14]. For example, various ATP-dependent disaggregases (molecules that break up molecular aggregates) and molecular motors are present in many RNA granules and are thus in a position to control the physical properties of condensates. Indeed, depletion of ATP increases the viscosity of stress granules and nucleoli [15]. Another example is the regulation of the size distribution of nucleoli by the actin cytoskeleton, the dynamics of which is itself controlled by ATP hydrolysis [16]. One suggested consequence of active processes is the suppression of Ostwald ripening. Classical coarsening theory predicts that only a single droplet remains following Ostwald ripening. However, in both the nucleus and cytoplasm there coexist several membrane-less organelles of the same basic composition, suggesting that there is some mechanism for suppressing Ostwald ripening. One potential candidate is the active regulation of liquid-liquid phase separation by ATP-driven enzymatic reactions that switch proteins between different conformational states (e.g., different levels of phosphorylation) [14,17–19]. Such a scheme has also been proposed as a mechanism for localized phase separation in *C. elegans* [20,21] and the organization of the centrosomes prior to cell division [22].

Theoretical models of the active suppression of Ostwald ripening have focused primarily on three-dimensional (3D) systems for which the LSW mean-field approximation can be applied [14,17–19]. The solute is assumed to exist in two different conformational states, an S state that does not phase separate and a P state that does. However, mean-field theory breaks down in the case of circular droplets in 2D systems, since the concentration around a droplet varies as $\ln R$ rather than R^{-1}, where R is the distance from the center of the droplet. Thus, more care must be taken in imposing far-field conditions, as previously shown for classical Ostwald ripening [23,24]. Mean-field theory also fails to capture finite-size effects. In this paper we use asymptotic methods to study the suppression of Ostwald ripening in a 2D or 3D solution undergoing active liquid-liquid phase separation. Assuming that droplets are well separated with mean separation L, we take $R/L = \epsilon\rho$ for $0 < \epsilon \ll 1$. We partition the region outside the droplets into a set of inner regions around each droplet together with an outer region where mean-field interactions occur. Matching the inner and outer solutions expressed as asymptotic expansions in $\nu = -1/\ln\epsilon$ (2D) or ϵ (3D), we derive leading-order conditions for the existence and stability of a multidroplet steady state. We also show how finite-size effects can be incorporated into the theory by including higher-order terms in the asymptotic expansion, which depend on the positions of the droplets and the boundary of the 2D or 3D domain.

We begin in Sec. II by briefly reviewing the mean-field approach to analyzing Ostwald ripening in 3D, before developing the asymptotic analysis of the corresponding problem in 2D. The latter uses a modified version of the formulation presented in Ref. [24]. We also highlight the relationship between the mean-field and asymptotic approaches in 3D. In Sec. III we apply the asymptotic method to the model for active phase separation introduced in Refs. [14,18]. In particular, we derive asymptotic expansions for the P-state and S-state concentrations inside and outside each droplet. We show that to leading order, the concentrations in a neighborhood of the ith droplet interface depend on the droplet radius ρ_i, the continuous S concentration Θ_i at the interface, the rates of switching α, β between the two conformational states, the width $\xi = \sqrt{D/(\alpha + \beta)}$ of the interfacial region (with D denoting the diffusion coefficient), and the total far-field concentration u_∞. We then use our results to calculate the effective P flux into each droplet, and obtain an equation for the rate of change of a droplet radius (on a relatively slow timescale).

In Sec. IV we derive conditions for the existence and stability of a multidroplet steady state. One crucial observation is that the stability of the steady state depends on fluctuations in Θ_i as well as ρ_i, with the former determined by requiring that continuity of the S flux is preserved by the perturbations. This establishes that stability depends on the local spatial gradient of the total solute concentration. That is, one cannot treat the total solute concentration in a neighborhood of a droplet as spatially uniform when the system is perturbed away from a multidroplet steady state. Indeed, the contribution from the total diffusive flux of the inner solution plays a crucial role in stabilizing the steady state, while ensuring continuity of the S flux across each droplet interface. Finally, following previous mean-field studies, we further develop the asymptotic analysis of 2D droplets in Sec. V by considering two particular regimes: a large-droplet regime ($\rho^*/\xi \gg 1$) and a small-droplet regime ($\rho^*/\xi \ll 1$), where ρ^* is the steady-state droplet radius.

We show that one difference between 2D and 3D in the small-droplet regime is that the in-flux has an additional logarithmic factor of the form $-1/\ln(\rho^*/\xi)$.

A final comment is in order. Membraneless structures such as P granules and nucleoli are 3D rather than 2D droplets, so it is not immediately clear why the analysis of 2D active phase separation is relevant within the context of biological condensates. However, it has recently been shown that active processes also occur within cell membranes, and contribute to various forms of phase separation [25–29]. One notable example is the clustering of curvature-inducing proteins that regulate cell shape. It should also be noted that understanding the behavior of active emulsions is of considerable interest within the wider physics community [19], and has many technological applications to the pharmaceutical, chemical, and food industries, where droplet size distribution and its stability needs to be controlled [30]. A number of applications involve thin films that can be treated as 2D domains.

II. OSTWALD RIPENING IN 2D AND 3D

A. Mean-field theory in 3D

Consider some macroscopic domain $\Omega \subset \mathbb{R}^3$ containing a collection of N microscopic droplets that are well separated from each other and whose total volume fraction is small. A no-flux boundary condition on $\partial\Omega$ ensures mass conservation. Represent each droplet as a sphere of radius R_i centered about $\mathbf{x}_i$, and assume that the dynamics of the droplet radii is much slower than the equilibration of the concentration profile (quasistatic approximation). The solute concentration ϕ exterior to the droplets then satisfies a simplified Mullins-Sekerka model:

$$\nabla^2\phi = 0, \quad \mathbf{r} \in \Omega \setminus \cup_{i=1}^{N} \Omega_i, \quad \partial_n\phi = 0 \text{ on } \partial\Omega, \quad (2.1a)$$

and

$$\phi = \phi_a\left(1 + \frac{\ell_c}{R_i}\right) \equiv \phi_a(R_i) \text{ on } \partial\Omega_i, \quad (2.1b)$$

where $\Omega_i = \{\mathbf{r} \in \Omega, |\mathbf{r} - \mathbf{x}_i| \leqslant R_i\}$ and ℓ_c is the capillary length. The boundary condition (2.1b) on the droplet interface is known as the Gibbs-Thomson law, and results in a net diffusive flux between droplets of different sizes. For example, suppose that there exist two droplets Σ_1 and Σ_2 with $R_2 < R_1$, see Fig. 1. From Eq. (2.1b), the concentration outside the smaller droplet will be higher than the concentration outside the larger droplet. Therefore, there will be a diffusive flux of solute from Σ_2 to Σ_1, resulting in the growth of Σ_1 at the expense of Σ_2. The same mechanism holds for multiple droplets, and results in a coarsening of the system in the form of Ostwald ripening [13].

The main approximation of LSW theory is to replace boundary effects and interactions between droplets by a mean field ϕ_∞ such that $\phi(\mathbf{x}) \approx \phi_\infty$ for $|\mathbf{r} - \mathbf{x}_i| \gg R_i$, $i = 1, \ldots, N$, and ϕ_∞ a constant to leading order. The quantity $\Delta = \phi_\infty - \phi_a$ is known as the supersaturation, and needs to be determined self-consistently from mass conservation. Hence, it will depend on the concentration of the original homogeneous solution and the sizes of the droplets. The mean-field approximation means that we can focus on a single droplet of radius R, say. Given the above assumptions, we
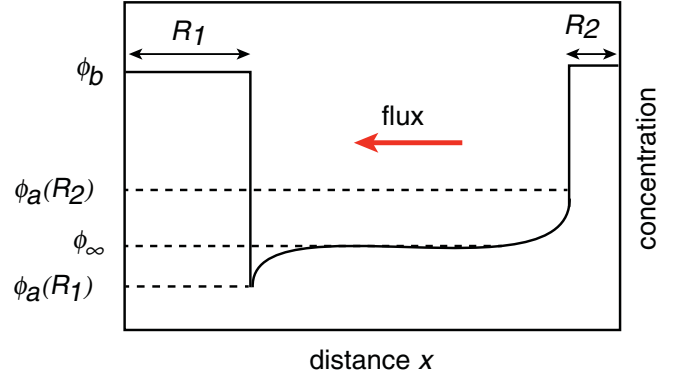

FIG. 1. Ostwald ripening. Schematic diagram showing the concentration profile as a function of x along the axis joining the centers of two well-separated droplets with different radii $R_1 > R_2$. The solute concentration $\phi_a(R_1)$ around the larger droplet is lower than the concentration $\phi_a(R_2)$ around the smaller droplet, resulting in a net diffusive flux from the small droplet to the large droplet. Here ϕ_∞ denotes the mean field of LSW theory.

take the concentration around the droplet to satisfy the radially symmetric diffusion equation

$$0 = \frac{D}{r^2}\frac{\partial}{\partial r}r^2\frac{\partial\phi}{\partial r}, \quad r > R, \quad (2.2)$$

supplemented by the boundary conditions

$$\phi(R) = \phi_a(R), \quad \phi(r) \to \phi_\infty \quad \text{as } r \to \infty. \quad (2.3)$$

Performing the change of variables $c(r) = r\phi(r)$, one finds that c satisfies the 1D diffusion equation so that

$$\phi(r) = \phi_\infty - \frac{R}{r}\left(\Delta - \frac{\phi_a\ell_c}{R}\right). \quad (2.4)$$

The corresponding diffusive flux of solute molecules entering the droplet at its interface is

$$J_R = D\nabla\phi(R) = \frac{D}{R}\left(\Delta - \frac{\phi_a\ell_c}{R}\right). \quad (2.5)$$

It follows that there exists a critical radius $R_c = \phi_a\ell_c/\Delta$ such that $J_R > 0$ when $R > R_c$ and the droplet grows due to a positive influx of solute molecules, see Fig. 1. On the other hand, small droplets with $R < R_c$ shrink as $J_R < 0$. [Within the context of the asymptotic methods developed below, Eq. (2.4) can be interpreted as the $O(1)$ inner solution for the solute concentration in a neighborhood of the droplet, which matches the mean-field concentration ϕ_∞ in the far-field limit.]

We can also write down a dynamical equation for the rate of change of the size of the droplet. When the radius increases by an amount dR, the volume increases by $dV = 4\pi R^2 dR$. Given that the expansion of the droplet involves the conversion of solute molecules from a low concentration $\phi_a(R)$ to a high concentration ϕ_b, it follows that the number of molecules required to enlarge the droplet by an amount dR is $[\phi_b - \phi_a(R)]dV$. These molecules are supplied by the flux at the interface. Hence, assuming that the change in radius occurs over an infinitesimal time dt, we have

$$4\pi R^2[\phi_b - \phi_a(R)]dR = 4\pi R^2 J_R dt,$$

which yields

$$\frac{dR}{dt} = \frac{D}{R[\phi_b - \phi_a(R)]}\left(\Delta - \frac{\phi_a \ell_c}{R}\right) \equiv \frac{\Gamma}{R}\left(\frac{1}{R_c} - \frac{1}{R}\right), \quad (2.6)$$

where

$$\Gamma = \frac{D\phi_a \ell_c}{[\phi_b - \phi_a(R)]} \approx \frac{D\phi_a \ell_c}{\phi_b}.$$

One gap in the above formulation of Ostwald ripening is how one determines the mean field ϕ_∞. In classical LSW theory, it is taken to be a constant in space and for each time t is determined by the constraint that the volume fraction of droplets is conserved. Assuming that there are N droplets at time t, we have

$$\frac{dR_i}{dt} = \frac{\Gamma}{R_i^2}\left(\frac{R_i}{R_c} - 1\right), \quad i = 1, \dots, N. \quad (2.7)$$

Multiplying both sides by R_i^2, summing over i, and imposing conservation of the volume fraction, $4\pi \sum_i R_i^3(t)/3 = $ constant, gives

$$R_c = \frac{1}{N}\sum_{i=1}^{N} R_i(t). \quad (2.8)$$

In other words,

$$\phi_\infty(t) = \phi_a\left[1 + \frac{\ell_c N}{\sum_{i=1}^{N} R_i(t)}\right]. \quad (2.9)$$

Equation (2.9) implies that $\phi_\infty(t)$ decreases as the mean radius increases. The latter will occur due to the disappearance of small droplets at the expense of larger droplets. As the saturation $\Delta(t) = \phi_\infty(t) - \phi_a$ decreases the critical radius R_c increases so that, ultimately, only a single droplet remains.

B. Asymptotic analysis in 2D

As we mentioned in the Introduction, classical LSW theory breaks down in the case of circular droplets in two-dimensional systems, since the concentration around a droplet varies as $\ln R$ rather than R^{-1}. Here we show how matched asymptotics can be used to handle the far-field behavior, following along similar lines to Ref. [24] (but with a modified choice of scalings). This will then be extended to active processes in Sec. III.

Consider N droplets of radii R_i and centers $\mathbf{x}_i$, $i = 1, \dots, N$, located in a bounded 2D domain $\Omega \subset \mathbb{R}^2$. The basic assumption of the asymptotic method is that the droplets are small and well separated. We fix length scales by setting the mean separation $L = 1$ and take $\ell_c = \epsilon$, $R_i = \epsilon \rho_i$ with $0 < \epsilon \ll 1$ and $\rho_i = O(1)$, and $|\mathbf{x}_i - \mathbf{x}_j| = O(1)$ for $j \neq i$. Let $\Omega_i = \{\mathbf{x} \in \Omega; |\mathbf{x} - \mathbf{x}_i| \leqslant \epsilon \rho_i\}$. The concentration ϕ outside the droplet satisfies the quasistatic diffusion equation

$$\nabla^2 \phi = 0, \quad \mathbf{x} \in \Omega \setminus \cup_{i=1}^{N} \Omega_i, \quad (2.10a)$$

supplemented by the boundary conditions

$$\partial_n \phi = 0 \text{ on } \partial\Omega, \quad \phi = \phi_a\left(1 + \frac{1}{\rho_i}\right) \text{ on } \partial\Omega_i. \quad (2.10b)$$
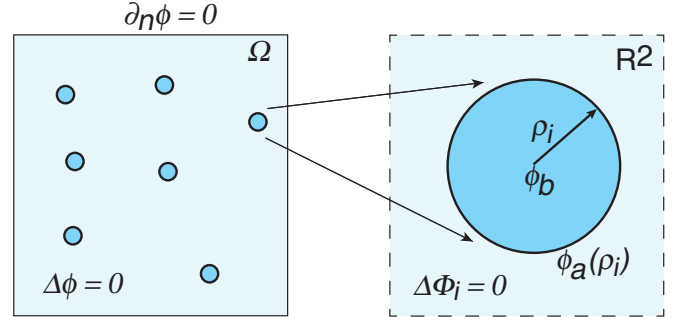

FIG. 2. Construction of the inner solution in terms of stretched coordinates $\mathbf{y} = \epsilon^{-1}(\mathbf{x} - \mathbf{x}_i)$, where $\mathbf{x}_i$ is the center of the ith droplet. Rescaled radius is ρ_i and the region outside the droplet is taken to be $\mathbb{R}^2$ rather than the bounded domain Ω. The concentration inside the droplet is given by the constant ϕ_b, with a discontinuity at the interface so that $\Phi_i(\rho_i^+) = \phi_a(\rho_i) = \phi_a(1 + 1/\rho_i)$.

First, consider the inner solution around the ith droplet,

$$\Phi_i(\mathbf{y}) = \phi(\mathbf{x}_i + \epsilon \mathbf{y}), \quad \mathbf{y} = \epsilon^{-1}(\mathbf{x} - \mathbf{x}_i),$$

where we have introduced stretched coordinates and replaced the domain Ω by $\mathbb{R}^2$, see Fig. 2. It follows that

$$\nabla_{\mathbf{y}}^2 \Phi_i = 0 \quad \text{for } \mathbf{y} \in \mathbb{R}^2 \setminus \Omega_i, \quad \Phi_i = \phi_a\left(1 + \frac{1}{\rho_i}\right) \text{ on } |\mathbf{y}| = \rho_i,$$

which can be expressed in polar coordinates as

$$\frac{1}{\rho}\frac{d}{d\rho}\rho\frac{d\Phi_i}{d\rho} = 0, \quad \rho_i < \rho < \infty, \quad \Phi_i(\rho_i) = \phi_a\left(1 + \frac{1}{\rho_i}\right).$$

The solution takes the form

$$\Phi_i(\rho) = \phi_a\left(1 + \frac{1}{\rho_i}\right) + \nu A_i(\nu)\ln(\rho/\rho_i), \quad (2.11)$$

where

$$\nu = -\frac{1}{\ln \epsilon}, \quad (2.12)$$

and $A_i(\nu)$ is some undetermined function of ν. The corresponding solution in the original coordinates is

$$\Phi_i(\mathbf{x}) = \phi_a\left(1 + \frac{1}{\rho_i}\right) + \nu A_i(\nu)\ln(|\mathbf{x} - \mathbf{x}_i|/\epsilon\rho_i). \quad (2.13)$$

The coefficients $A_i(\nu)$, $i = 1, \dots, N$, can be determined by matching the inner solutions with the corresponding outer solution (see below). The presence of the small parameter ν rather than ϵ in the matched asymptotic expansion is a common feature of strongly localized perturbations in 2D domains. It is well known that $\nu \to 0$ much more slowly than $\epsilon \to 0$. Hence, if one is interested in obtaining $O(\epsilon)$ accuracy, then it is necessary to sum over the logarithmic terms nonperturbatively. This can be achieved by matching the inner and outer solutions using Green's functions [31], which is equivalent to calculating the asymptotic solution for all terms of $O(\nu^k)$ for any k. We will follow this approach here, but for actual calculations we will expand in powers of ν. Note that 2D singular perturbation problems involving infinite logarithmic expansions arise in many other application areas, such as mean first passage time problems for Brownian
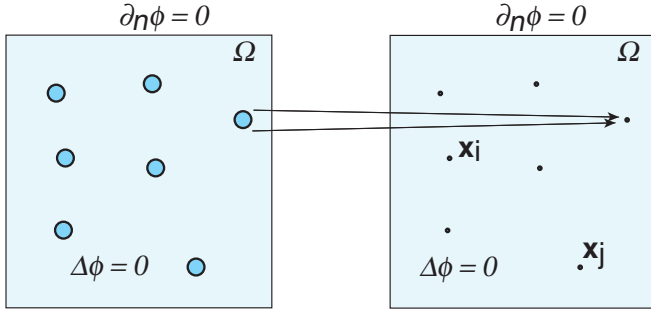
FIG. 3. Construction of the outer solution ϕ. Each droplet is shrunk to a single point. The outer solution can be expressed in terms of the corresponding modified Neumann Green's function and then matched with the inner solution Φ around each droplet.

motion in a domain with small traps [31–36] and diffusion-limited reaction rates in the case of small targets [37,38]. For a complementary approach to these types of problems see Refs. [39,40] and references therein.

The outer solution is obtained by treating each droplet as a point source or sink, see Fig. 3. The resulting time-independent diffusion equation takes the form

$$\nabla^2 \phi = 0, \quad \mathbf{x} \in \Omega \backslash \{\mathbf{x}_1, \dots, \mathbf{x}_N\}, \quad \partial_n \phi = 0, \quad \mathbf{x} \in \partial\Omega, \tag{2.14a}$$

together with the matching condition

$$\phi \sim \phi_a\left(1 + \frac{1}{\rho_j}\right) + A_j(\nu) + \nu A_j(\nu)[\ln|\mathbf{x} - \mathbf{x}_j| - \ln\rho_j] \tag{2.14b}$$

as $\mathbf{x} \to \mathbf{x}_j$. The next step is to introduce the 2D Neumann Green's function $G^{(2)}(\mathbf{x}, \mathbf{y})$, which is uniquely defined by

$$\nabla^2 G^{(2)} = \frac{1}{|\Omega|} - \delta(\mathbf{x} - \mathbf{y}), \quad \mathbf{x} \in \Omega \tag{2.15a}$$

and

$$\partial_n G^{(2)} = 0 \text{ on } \partial\Omega, \quad \int_\Omega G^{(2)} d\mathbf{x} = 0 \tag{2.15b}$$

for fixed $\mathbf{y}$. Note that $G^{(2)}$ can be decomposed as

$$G^{(2)}(\mathbf{x}, \mathbf{y}) = -\frac{\ln|\mathbf{x} - \mathbf{y}|}{2\pi} + R^{(2)}(\mathbf{x}, \mathbf{y}), \tag{2.16}$$

where $R^{(2)}$ is the regular part of the Green's function. We now make the ansatz

$$\phi(\mathbf{x}) \approx \phi_\infty - 2\pi\nu \sum_{i=1}^N A_i(\nu) G^{(2)}(\mathbf{x}, \mathbf{x}_i) \tag{2.17}$$

for $\mathbf{x} \notin \{\mathbf{x}_j, \ j = 1, \dots, N\}$ for some constant ϕ_∞. Observe that for $\mathbf{x} \notin \{\mathbf{x}_j, \ j = 1, \dots, N\}$,

$$\nabla^2 \phi(\mathbf{x}) \approx -2\pi\nu \sum_{i=1}^N A_i(\nu) \nabla^2 G^{(2)}(\mathbf{x}, \mathbf{x}_i) = -\frac{2\pi}{|\Omega|}\sum_{i=1}^N A_i(\nu).$$

Hence, the outer solution satisfies the steady-state diffusion equation if and only if

$$\sum_{i=1}^N A_i(\nu) = 0. \tag{2.18}$$

The latter is equivalent to imposing the condition that the total area occupied by droplets is conserved.

As $\mathbf{x} \to \mathbf{x}_j$,

$$\phi(\mathbf{x}) \to \phi_\infty + \nu A_j(\nu)\ln|\mathbf{x} - \mathbf{x}_j| - 2\pi\nu A_j(\nu)R^{(2)}(\mathbf{x}_j, \mathbf{x}_j)$$
$$- 2\pi\nu \sum_{i\neq j}^N A_i(\nu)G^{(2)}(\mathbf{x}_j, \mathbf{x}_i). \tag{2.19}$$

Comparison with the asymptotic limit in Eq. (2.14b) yields the self-consistency conditions

$$-[1 - \nu\ln\rho_j + 2\pi\nu R^{(2)}(\mathbf{x}_j, \mathbf{x}_j)]A_j(\nu)$$
$$- 2\pi\nu \sum_{i\neq j} A_i(\nu)G^{(2)}(\mathbf{x}_j, \mathbf{x}_i) = \phi_a\left(1 + \frac{1}{\rho_j}\right) - \phi_\infty \tag{2.20}$$

for $j = 1, \dots, N$. In particular, Eq. (2.20) can be rewritten as a matrix equation

$$\sum_{i=1}^N (\delta_{i,j} + \nu M_{ji})A_i(\nu) = \Delta - \frac{\phi_a}{\rho_j}, \tag{2.21}$$

with $\Delta = \phi_\infty - \phi_a$ the supersaturation and

$$M_{jj} = 2\pi R^{(2)}(\mathbf{x}_j, \mathbf{x}_j) - \ln\rho_j,$$
$$M_{ji} = 2\pi G^{(2)}(\mathbf{x}_j, \mathbf{x}_i), \ j \neq i. \tag{2.22}$$

We thus obtain the solution

$$A_i(\nu) = \sum_{j=1}^N [\mathbf{I} + \nu\mathbf{M}]_{ij}^{-1}\left(\Delta - \frac{\phi_a}{\rho_j}\right), \tag{2.23}$$

which is clearly nonperturbative with respect to ν.

It remains to determine the supersaturation Δ. Using the fact that $\int G^{(2)} d\mathbf{x} = 0$, it follows from Eq. (2.17) that

$$\phi_\infty = |\Omega|^{-1}\int_\Omega \phi(\mathbf{x})d\mathbf{x} = \overline{\phi}_{\text{out}},$$

where $\overline{\phi}_{\text{out}}$ is the mean concentration of solute outside the droplets. Early on during phase separation, the fractional volume of droplets is negligible so one can take $\phi_\infty = \phi_{\text{tot}}$, where ϕ_{tot} is the concentration of the homogeneous solution. However, as phase separation proceeds the volume fraction of droplets reaches a steady state so that Ostwald ripening preserves the total area occupied by droplets. The area-preserving condition (2.18) then holds, which combined with Eq. (2.23) implies that

$$\Delta = \phi_a \frac{\sum_{i,j=1}^N [\mathbf{I} + \nu\mathbf{M}]_{ij}^{-1}\rho_j^{-1}}{\sum_{i,j=1}^N [\mathbf{I} + \nu\mathbf{M}]_{ij}^{-1}}. \tag{2.24}$$

Hence, to leading order in ν,

$$\Delta \approx N^{-1}\sum_{i=1}^N \frac{\phi_a}{\rho_i} = \frac{\phi_a}{\rho_{\text{harm}}}, \tag{2.25}$$

where ρ_{harm} is the harmonic mean. This is one major difference from 3D, where Δ is given by the inverse of the arithmetic mean of the radii. Substituting the leading-order expression for the coefficients A_i into Eqs. (2.13) and (2.17) shows that the concentration outside droplets is

$$\phi(\mathbf{x}) = \phi_\infty - 2\pi\nu \sum_{i=1}^{N} \left(\Delta - \frac{\phi_a}{\rho_i} \right) G^{(2)}(\mathbf{x}, \mathbf{x}_i) + O(\nu^2),$$
(2.26)

and the inner solution near the ith droplet with $|\mathbf{x} - \mathbf{x}_i| = \epsilon\rho$ is

$$\Phi_i(\rho) = \phi_a\left(1 + \frac{1}{\rho_i}\right) + \nu\left(\Delta - \frac{\phi_a}{\rho_i}\right)\ln(\rho/\rho_i) + O(\nu^2).$$
(2.27)

Given the quasistatic solution for the concentration, we can now write down a dynamical equation for the rate of change of the size of each circular droplet along analogous lines to the 3D case. When the radius R_i increases by an amount dR_i, the area increases by $dA_i = 2\pi R_i dR_i$ and the number of molecules required to enlarge the droplet by an amount dR_i is $\phi_b dA_i$ [assuming for simplicity that $\phi_b \gg \phi(R_i)$]. These molecules are supplied by the flux at the interface. Hence after rescaling time by $t = \epsilon^2 \tau$, we have

$$\frac{d\rho_i}{d\tau} = \frac{D}{\phi_b}\Phi_i'(\rho_i) = \frac{D}{\phi_b}\frac{\nu A_i(\nu)}{\rho_i},$$
(2.28)

where $\Phi_i(\rho)$ is the inner solution (2.11). Now carrying out a perturbation expansion in ν shows that to leading order

$$\frac{d\rho_i}{d\tau} \approx \frac{D}{\phi_b}\frac{\nu}{\rho_i}\left(\Delta - \frac{\phi_a}{\rho_i}\right).$$
(2.29)

C. Asymptotic analysis in 3D

Although mean-field theory yields the leading-order dynamics of droplets in 3D, it is useful to see how higher-order corrections can be determined using asymptotic methods. These higher-order terms take into account finite-size effects associated with the boundary of the domain and the positions of the droplet centers. Consider Eqs. (2.10a) and (2.10b) with $\Omega \subset \mathbb{R}^3$ and Ω_i now a spherical droplet with radius ρ_i and center $\mathbf{x}_i \in \Omega$. Introducing stretched coordinates as in the 2D case, the inner solution around the ith droplet satisfies

$$\nabla_{\mathbf{y}}^2 \Phi_i = 0 \quad \text{for } \mathbf{y} \in \mathbb{R}^3 \backslash \Omega_i, \quad \Phi_i = \phi_a\left(1 + \frac{1}{\rho_i}\right) \quad \text{on } |\mathbf{y}| = \rho_i,$$

which can be expressed in spherical polar coordinates as

$$\frac{1}{\rho^2}\frac{d}{d\rho}\rho^2\frac{d\Phi_i}{d\rho} = 0, \quad \rho_i < \rho < \infty, \quad \Phi_i(\rho_i) = \phi_a\left(1 + \frac{1}{\rho_i}\right).$$

In the 2D case the far-field behavior of the inner solution is dominated by a logarithmic term, whose coefficient is determined by matching with the $O(\nu)$ outer solution. A major difference in the 3D case is that the inner solution vanishes as $\rho \to \infty$ unless its far-field behavior is explicitly matched

with the outer solution (whose leading-order term is the mean field ϕ_∞). This is achieved by expanding both the inner and outer solutions as power series in ϵ along analogous lines to Ref. [41]. We will proceed to $O(\epsilon)$.

First, expand the outer solution as

$$\phi(\mathbf{x}) = \phi_0(\mathbf{x}) + \epsilon\phi_1(\mathbf{x}) + \cdots,$$
(2.30)

with

$$\nabla^2 \phi_0 = 0, \quad \mathbf{x} \in \Omega, \quad \partial_n \phi_0 = 0, \quad \mathbf{x} \in \partial\Omega,$$
(2.31)

$$\nabla^2 \phi_1 = 0, \quad \mathbf{x} \in \Omega \backslash \{\mathbf{x}_1, \ldots, \mathbf{x}_N\}, \quad \partial_n \phi_1 = 0, \quad \mathbf{x} \in \partial\Omega,$$
(2.32)

and $\phi_1(\mathbf{x})$ singular as $\mathbf{x} \to \mathbf{x}_i$. If we now introduce a corresponding ϵ-expansion of the inner solution around the ith droplet

$$\Phi_i(\mathbf{y}) = \Phi_{i,0}(\mathbf{y}) + \epsilon\Phi_{i,1}(\mathbf{y}) + \cdots,$$
(2.33)

we then have

$$\nabla_{\mathbf{y}}^2 \Phi_{i,0} = 0 \quad \text{for } \mathbf{y} \in \mathbb{R}^3 \backslash \Omega_i,$$

$$\Phi_{i,0} = \phi_a\left(1 + \frac{1}{\rho_i}\right) \quad \text{on } |\mathbf{y}| = \rho_i,$$
(2.34)

$$\Phi_{i,0} \to \phi_0(\mathbf{x}_i) \quad \text{as } |\mathbf{y}| \to \infty,$$

and

$$\nabla_{\mathbf{y}}^2 \Phi_{i,1} = 0 \quad \text{for } \mathbf{y} \in \mathbb{R}^3 \backslash \Omega_i,$$

$$\Phi_{i,1} = 0 \quad \text{on } |\mathbf{y}| = \rho_i,$$
(2.35)

$$\Phi_{i,1} \to \phi_i^{\text{reg}} \quad \text{as } |\mathbf{y}| \to \infty,$$

Here ϕ_i^{reg} denotes the nonsingular part of $\phi_1(\mathbf{x})$ as $\mathbf{x} \to \mathbf{x}_i$. Finally, Eq. (2.32) is supplemented by the matching condition $\epsilon\phi_1 \sim \Phi_{i,0}$ as $\mathbf{x} \to \mathbf{x}_i$.

We now proceed iteratively. First, Eq. (2.31) has the mean-field solution $\phi_0(\mathbf{x}) = \phi_\infty$. It follows that $\Phi_{i,0}$ is given by the mean-field solution (2.4) in rescaled variables:

$$\Phi_{i,0}(\rho) = \phi_\infty - \frac{\rho_i}{\rho}\left(\Delta - \frac{\phi_a}{\rho_i}\right).$$
(2.36)

The outer solution ϕ_1 of Eq. (2.32) can now be obtained by introducing the 3D version of the Neumann Green's function, $G^{(3)}(\mathbf{x}, \mathbf{y})$, which is uniquely defined by Eqs. (2.15a) and (2.15b). In 3D the Green's function $G^{(3)}$ can be decomposed as

$$G^{(3)}(\mathbf{x}, \mathbf{y}) = \frac{1}{4\pi|\mathbf{x} - \mathbf{y}|} + R^{(3)}(\mathbf{x}, \mathbf{y}),$$
(2.37)

where $R^{(3)}$ is the regular part. The solution to Eq. (2.32) is then

$$\phi_1(\mathbf{x}) \approx -4\pi \sum_{i=1}^{N} \rho_i\left(\Delta - \frac{\phi_a}{\rho_i}\right)G^{(3)}(\mathbf{x}, \mathbf{x}_i)$$
(2.38)

for $\mathbf{x} \notin \{\mathbf{x}_j, \ j = 1, \ldots, N\}$ for some constant ϕ_∞. Observe that for $\mathbf{x} \notin \{\mathbf{x}_j, \ j = 1, \ldots, N\}$,

$$\nabla^2 \phi_1(\mathbf{x}) \approx -4\pi \sum_{i=1}^{N} \rho_i \left(\Delta - \frac{\phi_a}{\rho_i} \right) \nabla^2 G^{(3)}(\mathbf{x}, \mathbf{x}_i)$$

$$= -\frac{4\pi}{|\Omega|} \sum_{i=1}^{N} \rho_i \left(\Delta - \frac{\phi_a}{\rho_i} \right).$$

Hence, the $O(\epsilon)$ term in the expansion of the outer solution satisfies the steady-state diffusion equation if and only if $\sum_{i=1}^{N} (\rho_i \Delta - \phi_a) = 0$, which recovers Eq. (2.9) in rescaled variables. Finally, we can determine the $O(\epsilon)$ correction to the inner solution by substituting the regular part of $\phi_1(\mathbf{x})$ as $\mathbf{x} \to \mathbf{x}_i$ into Eq. (2.35):

$$\Phi_{i,1}(\rho) = \left(1 - \frac{\rho_i}{\rho} \right) \phi_i^{\text{reg}}, \tag{2.39}$$

with

$$\phi_i^{\text{reg}} = -4\pi \sum_{j \neq i} \rho_j \left(\Delta - \frac{\phi_a}{\rho_j} \right) G^{(3)}(\mathbf{x}_i, \mathbf{x}_j)$$

$$- 4\pi \rho_i \left(\Delta - \frac{\phi_a}{\rho_i} \right) R^{(3)}(\mathbf{x}_i, \mathbf{x}_i). \tag{2.40}$$

In Appendix A we list a few well-known Neumann Green's function in simple 2D and 3D geometries.

III. ACTIVE PHASE SEPARATION DRIVEN BY NONEQUILIBRIUM CHEMICAL REACTIONS

The model of a biological condensate introduced by Wurtz *et al.* [14,18] considers a ternary mixture consisting of two solute states, one phase separating (P) and the other soluble (S), together with the solvent or cytosol (C). It is assumed that switching between the states P and S occurs according to the chemical reactions

$$P \underset{h}{\overset{k}{\rightleftharpoons}} S,$$

where k and h are concentration-independent reaction rates. The latter reflects the nonequilibrium nature of the chemical reactions, in which detailed balance does not hold due to the phosphorylating action of ATP, say. Note that there is experimental evidence that the phase separation of intrinsically disordered proteins depends on their phosphorylation state [9]. As in Sec. II, we will consider N small droplets with radii R_i and positions $\mathbf{x}_i \in \Omega \subset \mathbb{R}^d$, $d = 2, 3$. Denoting the concentrations of P and S molecules inside the ith droplet by $\widehat{\phi}_i$ and $\widehat{\psi}_i$, respectively, we have the quasistatic equations

$$D\nabla^2 \widehat{\phi}_i - k\widehat{\phi}_i + h\widehat{\psi}_i = 0, \tag{3.1a}$$

$$D\nabla^2 \widehat{\psi}_i + k\widehat{\phi}_i - h\widehat{\psi}_i = 0, \quad \mathbf{x} \in \Omega_i, \tag{3.1b}$$

together with the boundary condition s

$$\widehat{\phi}_i = \phi_b, \quad \widehat{\psi}_i = \Theta_i \text{ on } \partial\Omega_i, \tag{3.1c}$$

with Θ_i to be determined (see Sec. III C). For simplicity, both solute species are assumed to have the same diffusion
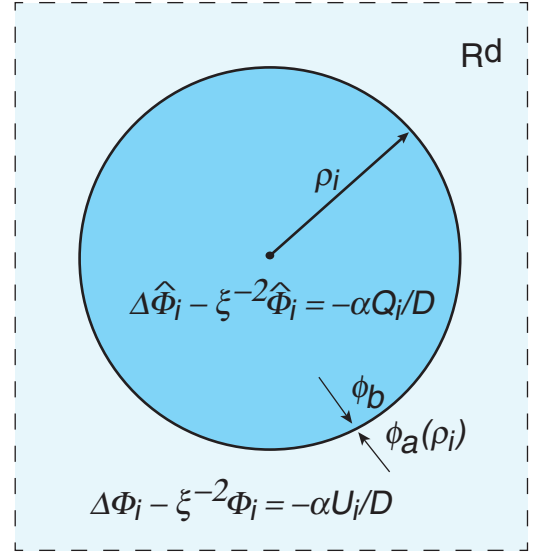

FIG. 4. Interior and exterior droplet regions in stretched coordinates. The P concentration satisfies an inhomogeneous modified Helmholtz equation with length constant $\xi = \sqrt{D/(\alpha + \beta)}$ and U the total solute concentration (including molecules in the P and S states). The total concentration within the droplet is a constant Q_i. The P-state concentration is discontinuous at the interface with $\widehat{\Phi}_i(\rho_i) = \phi_b$ and $\Phi_i(\rho_i) = \phi_a(\rho_i) \equiv \phi_a(1 + 1/\rho_i)$. On the other hand the S-state concentration is continuous at the interface.

coefficient D. Similarly, denoting the corresponding concentrations outside the droplets by ϕ and ψ, respectively, we have

$$D\nabla^2 \phi - k\phi + h\nu = 0, \tag{3.2a}$$

$$D\nabla^2 \psi + k\phi - h\psi = 0, \quad \mathbf{x} \in \Omega \backslash \cup_{i=1}^{N} \Omega_i, \tag{3.2b}$$

supplemented by the boundary and continuity conditions

$$\partial_n \phi = 0 = \partial_n \psi \quad \text{on } \partial\Omega,$$

$$\phi = \phi_a \left(1 + \frac{\ell_c}{R_i} \right), \quad \psi = \Theta_i \quad \text{on } \partial\Omega_i. \tag{3.2c}$$

Again we will fix the length scale by setting $L = 1$ such that $\ell_c = \epsilon$ and $R_i = \epsilon\rho_i$.

A. Droplet interior

Introduce stretched coordinates inside the ith droplet,

$$\widehat{\Phi}_i(\mathbf{y}) = \widehat{\phi}_i(\mathbf{x}_i + \epsilon\mathbf{y}), \quad \widehat{\Psi}_i(\mathbf{y}) = \widehat{\psi}_i(\mathbf{x}_i + \epsilon\mathbf{y})$$

for $\mathbf{y} = \epsilon^{-1}(\mathbf{x} - \mathbf{x}_i)$ and $|\mathbf{y}| \leqslant \rho_i$, see Fig. 4. Equation (3.1) then take the form

$$D\nabla_{\mathbf{y}}^2 \widehat{\Phi}_i - \beta\widehat{\Phi}_i + \alpha\widehat{\Psi}_i = 0, \tag{3.3a}$$

$$D\nabla_{\mathbf{y}}^2 \widehat{\Psi}_i + \beta\widehat{\Phi}_i - \alpha\widehat{\Psi}_i = 0, \quad |\mathbf{y}| \leqslant \rho_i, \tag{3.3b}$$

where we have introduced the rescaled reaction rates

$$\alpha = \epsilon^2 h, \quad \beta = \epsilon^2 k,$$

supplemented by the boundary conditions $\widehat{\Phi}_i = \phi_b$ and $\widehat{\Psi}_i = \Theta_i$ for $|\mathbf{y}| = \rho_i$. Adding Eqs. (3.3) and (3.3b), we have

$$D\nabla_{\mathbf{y}}^2 (\widehat{\Phi}_i + \widehat{\Psi}_i) = 0, \quad |\mathbf{y}| \leqslant \rho_i. \tag{3.4}$$

Introducing polar coordinates shows that

$$\widehat{\Phi}_i(\rho) + \widehat{\Psi}_i(\rho) = \begin{cases} Q_i + \widehat{Q}_i \ln \rho & \text{(2D)} \\ Q_i + \widehat{Q}_i/\rho & \text{(3D)} \end{cases}$$

for $0 \leqslant \rho \leqslant \rho_i$. In order to avoid the singularity at $\rho = 0$ we set $\widehat{Q}_i = 0$, which implies that $\widehat{\Phi}_i(\rho) + \widehat{\Psi}_i(\rho) = Q_i \equiv \phi_b + \Theta_i$ is a constant inside the droplet. This then allows us to decouple Eqs. (3.3) and (3.3b) such that $\widehat{\Phi}_i$ satisfies the modified Helmholtz equation

$$\nabla_{\mathbf{y}}^2 \widehat{\Phi}_i - \xi^{-2} \widehat{\Phi}_i = -\frac{\alpha(\phi_b + \Theta_i)}{D}, \quad 0 \leqslant \rho \leqslant \rho_i, \quad (3.5)$$

where we have introduced the new length scale

$$\xi = \sqrt{\frac{D}{\alpha + \beta}}. \quad (3.6)$$

1. Two-dimensional droplets

For a circular droplet, Eq. (3.5) can be written in polar coordinates

$$\frac{1}{\rho} \frac{d}{d\rho} \rho \frac{d\widehat{\Phi}_i}{d\rho} - \xi^{-2} \widehat{\Phi}_i = -\frac{\alpha(\phi_b + \Theta_i)}{D}, \quad 0 \leqslant \rho \leqslant \rho_i, \quad (3.7)$$

where Eq. (3.7) has the nonsingular solution

$$\widehat{\Phi}_i(\rho) = c_i I_0(\rho/\xi) + \frac{\alpha[\phi_b + \Theta_i]}{\alpha + \beta}. \quad (3.8)$$

Imposing the boundary condition $\Phi_i(\rho_i) = \phi_b$ then determines the coefficient c_i:

$$\widehat{\Phi}_i(\rho) = \left(\frac{\beta}{\alpha + \beta}\phi_b - \frac{\alpha\Theta_i}{\alpha + \beta}\right)\frac{I_0(\rho/\xi)}{I_0(\rho_i/\xi)} + \frac{\alpha[\phi_b + \Theta_i]}{\alpha + \beta}. \quad (3.9)$$

2. Three-dimensional droplets

Similarly, using spherical polar coordinates in 3D, we have

$$\frac{1}{\rho^2} \frac{d}{d\rho} \rho^2 \frac{d\widehat{\Phi}_i}{d\rho} - \xi^{-2} \widehat{\Phi}_i = -\frac{\alpha(\phi_b + \Theta_i)}{D}, \quad 0 \leqslant \rho \leqslant \rho_i, \quad (3.10)$$

Performing the change of variables $c_i(\rho) = \rho\widehat{\Phi}_i(\rho)$, we have

$$\frac{d^2 c_i}{d\rho^2} - \xi^{-2} c_i = -\rho\frac{\alpha(\phi_b + \Theta_i)}{D}, \quad 0 \leqslant \rho \leqslant \rho_i. \quad (3.11)$$

The solution is thus

$$\widehat{\Phi}_i(\rho) = \left(\phi_b - \frac{\alpha[\phi_b + \Theta_i]}{\alpha + \beta}\right)\frac{\rho_i}{\rho}\frac{\sinh(\rho/\xi)}{\sinh(\rho_i/\xi)} + \frac{\alpha[\phi_b + \Theta_i]}{\alpha + \beta}. \quad (3.12)$$

The sinh function is required for the inner solution so that it is nonsingular at $\rho = 0$

B. Droplet exterior

Let us now turn to the region exterior to droplets. First, adding Eqs. (3.2a) and (3.2b) and setting $\phi + \psi = u$, we have

$$D\nabla^2 u = 0, \quad \mathbf{x} \in \Omega \setminus \cup_{i=1}^{N} \Omega_i, \quad \partial_n u = 0 \text{ on } \partial\Omega \quad (3.13a)$$

and

$$u = \mathcal{U}_i \equiv \Theta_i + \phi_a\left(1 + \frac{1}{\rho_i}\right) \text{ on } \partial\Omega_i. \quad (3.13b)$$

Equation (3.13a) can be analyzed along almost identical lines to Secs. II B and II C by partitioning the exterior domain into an outer region and a set of N inner regions. Denote the resulting outer and inner solutions by u and U_i, respectively. Given these solutions, we define the inner solutions for the P and S concentrations according to

$$\Phi_i(\mathbf{y}) = \phi_i(\mathbf{x}_i + \epsilon\mathbf{y}), \quad \Psi_i(\mathbf{y}) = \psi_i(\mathbf{x}_i + \epsilon\mathbf{y})$$

for $\mathbf{y} = \epsilon^{-1}(\mathbf{x} - \mathbf{x}_i)$ and $\rho_i < |\mathbf{y}| < \infty$, see Fig. 4. It follows that $\Psi_i(\mathbf{y}) = U_i(\mathbf{y}) - \Phi_i(\mathbf{y})$ with Φ_i satisfying the inhomogeneous modified Helmholtz equation

$$\nabla_{\mathbf{y}}^2 \Phi_i - \xi^{-2} \Phi_i = -\frac{\alpha U_i(\mathbf{y})}{D}, \quad |\mathbf{y}| \geqslant \rho_i, \quad (3.14a)$$

and

$$\Phi_i = \phi_a\left(1 + \frac{1}{\rho_i}\right), \quad |\mathbf{y}| = \rho_i. \quad (3.14b)$$

(We focus on the inner solutions, since these determine the fluxes at the interface.) Since $\nabla_{\mathbf{y}}^2 U_i = 0$, the solution of Eq. (3.14a) is of the general form

$$\Phi_i(\mathbf{y}) = \left\{\phi_a\left(1 + \frac{1}{\rho_i}\right) - \frac{\alpha\mathcal{U}_i}{\alpha + \beta}\right\}C_i(\mathbf{y}) + \frac{\alpha U_i(\rho)}{\alpha + \beta}, \quad (3.15)$$

where $C_i(\mathbf{y})$ is the solution of the homogeneous modified Helmholtz equation

$$\nabla_{\mathbf{y}}^2 C_i - \xi^{-2} C_i = 0 \quad \text{for } |\mathbf{y}| \geqslant \rho_i,$$
$$C_i = 1 \quad \text{on } |\mathbf{y}| = \rho_i. \quad (3.16)$$

1. Two-dimensional droplets

In the case of 2D droplets, summing up all logarithmic singularities yields the inner and outer solutions

$$U_i(\rho) = \mathcal{U}_i + \nu B_i(\nu) \ln(\rho/\rho_i) \quad (3.17)$$

for $\rho_i < \rho < \infty$, and

$$u(\mathbf{x}) = u_\infty - 2\pi\nu \sum_{i=1}^{N} B_i(\nu) G^{(2)}(\mathbf{x}, \mathbf{x}_i) \quad (3.18)$$

for $\mathbf{x} \notin \{\mathbf{x}_j, \ j = 1, \dots, N\}$. The coefficients $B_i(\nu)$ are given by

$$B_i(\nu) = \sum_{j=1}^{N} [\mathbf{I} + \nu\mathbf{M}]_{ij}^{-1}(u_\infty - \mathcal{U}_j) \approx u_\infty - \mathcal{U}_i \quad (3.19)$$

and

$$u_\infty = \frac{\sum_{i,j=1}^{N} [\mathbf{I} + \nu\mathbf{M}]_{ij}^{-1}\mathcal{U}_j}{\sum_{i,j=1}^{N} [\mathbf{I} + \nu\mathbf{M}]_{ij}^{-1}} \approx \phi_a\left(1 + \frac{1}{\rho_{\text{harm}}}\right) + \overline{\Theta} \quad (3.20)$$

with $\overline{\Theta} = N^{-1} \sum_{i=1}^{N} \Theta_i$. Now solving the modified Helmholtz equation (3.16) in polar coordinates yields

$$\Phi_i(\rho) = \left\{ \phi_a \left(1 + \frac{1}{\rho_i} \right) - \frac{\alpha \mathcal{U}_i}{\alpha + \beta} \right\} \frac{K_0(\rho/\xi)}{K_0(\rho_i/\xi)} + \frac{\alpha U_i(\rho)}{\alpha + \beta}, \tag{3.21}$$

where $K_0(z)$ is the modified Bessel function of zeroth order that is nonsingular at infinity. However, it has a logarithmic singularity at $z = 0$. Note that the inner solution automatically matches the outer solution

$$\phi(\mathbf{x}) \approx \frac{\alpha}{\alpha + \beta} u(\mathbf{x}), \quad \psi(\mathbf{x}) \approx \frac{\beta}{\alpha + \beta} u(\mathbf{x}), \tag{3.22}$$

since $K_0(\rho/\xi) \to 0$ as $\rho \to \infty$.

2. Three-dimensional droplets

Similarly, in the case of 3D droplets, the inner solution U_i is given by

$$U_i(\rho) = u_\infty - \frac{\rho_i}{\rho} [u_\infty - \mathcal{U}_i] + \epsilon \left(1 - \frac{\rho_i}{\rho} \right) \Lambda_i(\boldsymbol{\rho}, \boldsymbol{\Theta}) + O(\epsilon^2), \tag{3.23}$$

with $\boldsymbol{\rho} = (\rho_1, \ldots, \rho_N)$, $\boldsymbol{\Theta} = (\Theta_1, \ldots, \Theta_N)$,

$$\Lambda_i(\boldsymbol{\rho}, \boldsymbol{\Theta}) = -4\pi \sum_{j \neq i} \rho_j [u_\infty - \mathcal{U}_j] G^{(3)}(\mathbf{x}_i, \mathbf{x}_j)$$
$$- 4\pi \rho_i [u_\infty - \mathcal{U}_i] R^{(3)}(\mathbf{x}_i, \mathbf{x}_i) + O(\epsilon^2), \tag{3.24}$$

and $\mathcal{U}_i$ defined in Eq. (3.13b). The corresponding outer solution is

$$u(\mathbf{x}) = u_\infty - 4\pi \epsilon \sum_{i=1}^{N} \rho_i [u_\infty - \mathcal{U}_i] G^{(3)}(\mathbf{x}, \mathbf{x}_i) + O(\epsilon^2). \tag{3.25}$$

Finally, solving the modified Helmholtz equation (3.16) in spherical polar coordinates yields

$$\Phi_i(\rho) = \left\{ \phi_a \left(1 + \frac{1}{\rho_i} \right) - \frac{\alpha \mathcal{U}_i}{\alpha + \beta} \right\} \frac{\rho_i}{\rho} e^{-(\rho - \rho_i)/\xi} + \frac{\alpha U_i(\rho)}{\alpha + \beta}. \tag{3.26}$$

C. Interfacial fluxes and droplet dynamics

As in the classical theory of Ostwald ripening, the rate of change of the radius ρ_i (in rescaled variables) is given by the jump in the flux normal to the interface at $\rho = \rho_i$:

$$\frac{d\rho_i}{d\tau} = \frac{1}{\phi_b} [J_{i,+} - J_{i,-}], \tag{3.27}$$

where we have rescaled time according to $t = \epsilon^2 \tau$, which is consistent with the rescaling of the reaction rates, and introduced the P fluxes

$$J_{i,-} = D \left. \frac{d\widehat{\Phi}_i}{d\rho} \right|_{\rho = \rho_i^-} \equiv J_-(\rho_i, \Theta_i), \tag{3.28a}$$

$$J_{i,+} = D \left. \frac{d\Phi_i}{d\rho} \right|_{\rho = \rho_i^+} \equiv J_+(\rho_i, \Theta_i) + j_i(\boldsymbol{\rho}, \boldsymbol{\Theta}), \tag{3.28b}$$

Using Eq. (3.15), we have further decomposed the exterior flux into two components:

$$J_+(\rho_i, \Theta_i) = D \left\{ \phi_a \left(1 + \frac{1}{\rho_i} \right) - \frac{\alpha \mathcal{U}_i}{\alpha + \beta} \right\} \left. \frac{dC_i}{d\rho} \right|_{\rho = \rho_i^+}, \tag{3.28c}$$

where $C_i(\rho_i)$ is the solution to Eq. (3.16) in polar or spherical polar coordinates, and

$$j_i(\boldsymbol{\rho}, \boldsymbol{\Theta}) = \frac{\alpha}{\alpha + \beta} D U_i'(\rho_i). \tag{3.28d}$$

Note that if one includes higher-order terms in the asymptotic expansion of the inner solution U_i, then the flux j_i depends on all radii $\boldsymbol{\rho} = (\rho_1, \ldots, \rho_N)$ and all concentrations $\boldsymbol{\Theta} = (\Theta_1, \ldots, \Theta_N)$, see Appendix B. Hence, the asymptotic analysis is crucial for determining the local flux j_i, which is proportional to the gradient U' of the total solute concentration. As we will see in Sec. IV, although this flux vanishes when the system is in a multidroplet steady state, it has nonzero fluctuations that contribute to the stability of the steady state.

The N unknown constants Θ_i can now be determined by imposing continuity of the S flux at the interface. More specifically, let

$$\widetilde{J}_{i,-} = D \left. \frac{d\widehat{\Psi}_i}{d\rho} \right|_{\rho = \rho_i^-}, \quad \widetilde{J}_{i,+} = D \left. \frac{d\Psi_i}{d\rho} \right|_{\rho = \rho_i^+}. \tag{3.29}$$

Since

$$\widehat{\Psi}_i(\rho) = \phi_b + \Theta_i - \widehat{\Phi}_i(\rho), \quad \text{for } 0 < \rho < \rho_i,$$
$$\Psi_i(\rho) = U_i(\rho) - \Phi_i(\rho) \quad \text{for } \rho > \rho_i, \tag{3.30}$$

it follows that

$$\widetilde{J}_{i,-} = -J_-(\rho_i, \Theta_i),$$
$$\widetilde{J}_{i,+} = \frac{\beta}{\alpha} j_i(\boldsymbol{\rho}, \boldsymbol{\Theta}) - J_+(\rho_i, \Theta_i). \tag{3.31}$$

Continuity of the S flux at the interface $\rho = \rho_i$ then requires

$$J_+(\rho_i, \Theta_i) - J_-(\rho_i, \Theta_i) = \frac{\beta}{\alpha} j_i(\boldsymbol{\rho}, \boldsymbol{\Theta}). \tag{3.32}$$

The various contributions to the P flux and S flux across a droplet interface are illustrated in Fig. 5.

1. Two-dimensional droplets

From Eqs. (3.9), (3.17), and (3.21) and the definitions of the fluxes in Eq. (3.28), we find that for circular droplets

$$J_+(\rho, \Theta) = \frac{D}{\xi} \left\{ \frac{\beta}{\alpha + \beta} \phi_a \left(1 + \frac{1}{\rho} \right) - \frac{\alpha \Theta}{\alpha + \beta} \right\} \frac{K_0'(\rho/\xi)}{K_0(\rho/\xi)}, \tag{3.33a}$$

$$J_-(\rho, \Theta) = \frac{D}{\xi} \left(\frac{\beta}{\alpha + \beta} \phi_b - \frac{\alpha \Theta}{\alpha + \beta} \right) \frac{I_0'(\rho/\xi)}{I_0(\rho/\xi)}, \tag{3.33b}$$

and

$$j_i(\boldsymbol{\rho}, \boldsymbol{\Theta}) = \frac{\alpha}{\alpha + \beta} \frac{\nu D B_i(\boldsymbol{\rho}, \boldsymbol{\Theta})}{\rho_i}. \tag{3.33c}$$

The coefficients B_i, which are given by Eq. (3.19), have an $O(\nu)$ dependence on all radii $\boldsymbol{\rho} = (\rho_1, \ldots, \rho_N)$ and all concentrations $\boldsymbol{\Theta} = (\Theta_1, \ldots, \Theta_N)$.
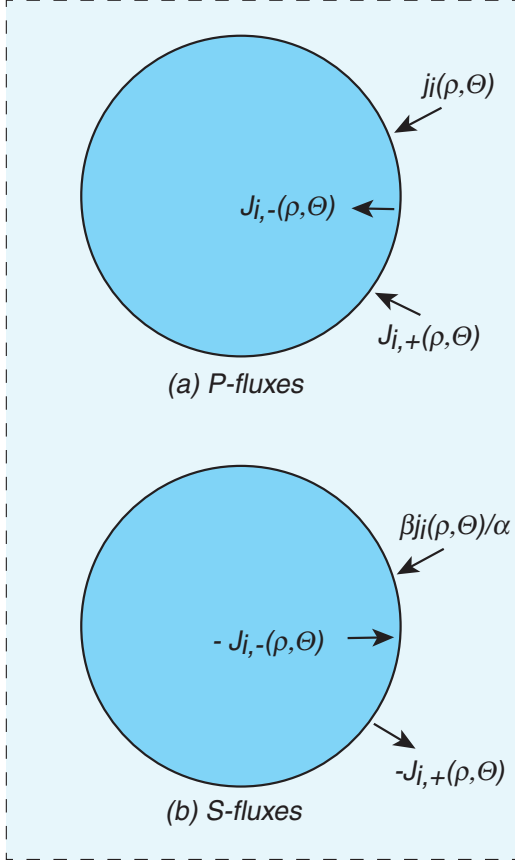
FIG. 5. (a) Various P fluxes crossing the ith droplet interface. There is one outward current $J_{i,-}(\rho, \Theta)$ and two inward currents $J_{i,+}(\rho, \Theta)$ and $j_i(\rho, \Theta)$, where ρ is the droplet radius and Θ is the continuous S concentration at the interface. The current j_i depends on the local gradient U_i' of the total solute concentration outside the droplet. The fluxes balance at the steady-state solution (ρ^*, Θ^*) with $j_i(\rho^*, \Theta^*) = 0$. (b) Corresponding S fluxes. The net S flux is continuous across the interface.

2. Three-dimensional droplets

From Eqs. (3.12), (3.23), and (3.26) and the definitions of the fluxes in Eq. (3.28), we find that for spherical droplets

$$J_+(\rho, \Theta) = \frac{D}{\xi}\left\{\frac{\alpha\Theta}{\alpha+\beta} - \frac{\beta}{\alpha+\beta}\phi_a\left(1 + \frac{1}{\rho}\right)\right\}\left(1 + \frac{\xi}{\rho}\right),$$
(3.34a)

$$J_-(\rho, \Theta) = \frac{D}{\xi}\left(\frac{\beta}{\alpha+\beta}\phi_b - \frac{\alpha\Theta}{\alpha+\beta}\right)\left[\coth(\rho/\xi) - \frac{\xi}{\rho}\right],$$
(3.34b)

and

$$j_i(\boldsymbol{\rho}, \boldsymbol{\Theta}) = \frac{\alpha}{\alpha+\beta}\frac{D}{\rho_i}\left[u_\infty - \Theta_i - \phi_a\left(1 + \frac{1}{\rho_i}\right)\right]$$
$$+ \epsilon \frac{\alpha}{\alpha+\beta}\frac{D}{\rho_i}\Lambda_i(\boldsymbol{\rho}, \boldsymbol{\Theta}) + O(\epsilon^2).$$
(3.34c)

The term $\Lambda_i(\boldsymbol{\rho}, \boldsymbol{\Theta})$, which is given by Eq. (3.24), depends on all radii $\boldsymbol{\rho} = (\rho_1, \ldots, \rho_N)$ and all concentrations $\boldsymbol{\Theta} = (\Theta_1, \ldots, \Theta_N)$.

IV. EXISTENCE AND STABILITY OF MULTIDROPLET STATES

We are interested in the existence and stability of a steady state $\rho_i = \rho^*$ and $\Theta_i = \Theta^*$ for all $i = 1, \ldots, N$. A major observation is that Θ^* and ρ^* are related according to

$$\Theta^* + \phi_a\left(1 + \frac{1}{\rho^*}\right) = u_\infty.$$
(4.1)

This means that the far-field and near-field total solute concentrations are the same, that is, the total exterior concentration is spatially uniform. Hence,

$$j_i(\boldsymbol{\rho}^*, \boldsymbol{\Theta}^*) = 0 \quad \text{for all } i = 1, \ldots N,$$

and we obtain the P-flux balance condition

$$J_+(\rho^*, \Theta^*) = J_-(\rho^*, \Theta^*).$$
(4.2)

Continuity of the S flux at the interface then immediately follows from Eq. (3.32).

The local stability of the multidroplet steady state can be determined by considering perturbations of the form $\rho_i = \rho^* + \delta\rho_i$, $\Theta_i = \Theta^* + \delta\Theta_i$, such that u_∞ is unchanged. The corresponding P flux into the ith droplet is then

$$\delta J_i = \left[\frac{\partial J_+}{\partial \rho^*} - \frac{\partial J_-}{\partial \rho^*}\right]\delta\rho_i + \left[\frac{\partial J_+}{\partial \Theta^*} - \frac{\partial J_-}{\partial \Theta^*}\right]\delta\Theta_i$$
$$+ \sum_{l=1}^N \left\{\frac{\partial j_i}{\partial \rho_l}\delta\rho_l + \frac{\partial j_i}{\partial \Theta_l}\delta\Theta_l\right\},$$
(4.3)

where all derivatives are evaluated at the steady state. However, there is a relationship between the perturbations $\delta\boldsymbol{\Theta}$ and $\delta\boldsymbol{\rho}$, since continuity of the S fluxes at the interface must be preserved. From Eq. (3.32), this takes the form

$$\frac{\beta}{\alpha}\sum_{l=1}^N \left\{\frac{\partial j_i}{\partial \rho_l}\delta\rho_l + \frac{\partial j_i}{\partial \Theta_l}\delta\Theta_l\right\}$$
$$= \left[\frac{\partial J_+}{\partial \rho^*} - \frac{\partial J_-}{\partial \rho^*}\right]\delta\rho_i + \left[\frac{\partial J_+}{\partial \Theta^*} - \frac{\partial J_-}{\partial \Theta^*}\right]\delta\Theta_i.$$
(4.4)

Introducing the scalar and matrix functions

$$\mathcal{P} = \frac{\partial J_+}{\partial \rho^*} - \frac{\partial J_-}{\partial \rho^*},$$
(4.5a)

$$\mathcal{Q} = \frac{\partial J_+}{\partial \Theta^*} - \frac{\partial J_-}{\partial \Theta^*},$$
(4.5b)

$$P_{il} = \frac{\partial j_i}{\partial \rho_l}(\boldsymbol{\rho}^*, \boldsymbol{\Theta}^*), \quad Q_{il} = \frac{\partial j_i}{\partial \Theta_l}(\boldsymbol{\rho}^*, \boldsymbol{\Theta}^*),$$
(4.5c)

Eqs. (4.3) and (4.4) can be rewritten as

$$\delta J_i = \frac{\beta+\alpha}{\beta}\left\{\left[\frac{\partial J_+}{\partial \rho^*} - \frac{\partial J_-}{\partial \rho^*}\right]\delta\rho_i + \left[\frac{\partial J_+}{\partial \Theta^*} - \frac{\partial J_-}{\partial \Theta^*}\right]\delta\Theta_i\right\},$$
(4.6)

with

$$\delta\Theta_i = -\sum_{l,k=1}^N \left[\mathcal{Q}\mathbf{I} - \frac{\beta}{\alpha}\mathbf{Q}\right]_{il}^{-1}\left[\mathcal{P}\mathbf{I} - \frac{\beta}{\alpha}\mathbf{P}\right]_{lk}\delta\rho_k.$$
(4.7)

Considerable simplification occurs if we only keep the leading-order terms in the asymptotic expansion of the fluxes

j_i. In the case of 3D droplets, substituting Eq. (3.13b) into (3.34) shows that to $O(1)$

$$P_{il} = \frac{\alpha}{\alpha + \beta} \frac{D\phi_a}{\rho^{*3}} \delta_{i,l} + O(\epsilon), \tag{4.8}$$

$$Q_{il} = -\frac{\alpha}{\alpha + \beta} \frac{D}{\rho^*} \delta_{i,l} + O(\epsilon). \tag{4.9}$$

Similarly, keeping the leading-order term in the ν series expansion of the coefficients $B_i(\nu)$ in Eq. (3.33),

$$P_{il} = \frac{\alpha}{\alpha + \beta} \frac{\nu D\phi_a}{\rho^{*3}} \delta_{i,l} + O(\nu^2),$$

$$Q_{il} = -\frac{\alpha}{\alpha + \beta} \frac{\nu D}{\rho^*} \delta_{i,l} + O(\nu^2). \tag{4.10}$$

Substituting these approximations into Eqs. (4.3) and (4.4) yields to leading order

$$\delta J_i \approx \Gamma_d \left\{ \frac{1}{\rho^*} \left[\frac{\partial J_+}{\partial \rho^*} - \frac{\partial J_-}{\partial \rho^*} \right] + \frac{\phi_a}{\rho^{*3}} \left[\frac{\partial J_+}{\partial \Theta^*} - \frac{\partial J_-}{\partial \Theta^*} \right] \right\} \delta \rho_i \tag{4.11}$$

for all $i = 1, \dots, N$ and $d = 2, 3$, with

$$\Gamma_2 = \nu D \left[\frac{\partial J_+}{\partial \Theta^*} - \frac{\partial J_-}{\partial \Theta^*} + \frac{\beta}{\alpha + \beta} \frac{\nu D}{\rho^*} \right]^{-1}, \tag{4.12a}$$

$$\Gamma_3 = D \left[\frac{\partial J_+}{\partial \Theta^*} - \frac{\partial J_-}{\partial \Theta^*} + \frac{\beta}{\alpha + \beta} \frac{D}{\rho^*} \right]^{-1}. \tag{4.12b}$$

Finally, requiring that δJ_i and $\delta \rho_i$ have opposite signs leads to the $O(1)$ stability condition

$$\frac{\phi_a}{\rho^{*2}} \left[\frac{\partial J_+}{\partial \Theta^*} - \frac{\partial J_-}{\partial \Theta^*} \right] + \left[\frac{\partial J_+}{\partial \rho^*} - \frac{\partial J_-}{\partial \rho^*} \right] < 0, \tag{4.13}$$

since one finds that $\Gamma_d > 0$. The stability condition (4.13) reduces to one obtained previously for 3D systems [14,18,19], under the mean-field approximation

$$\Theta_i + \phi_a \left(1 + \frac{1}{\rho_i} \right) = u_\infty$$

for all perturbations of the multidroplet steady state. However, the above condition does not preserve continuity of the S flux across the interface, and thus fails to capture the physical mechanism for stabilizing the steady state. In addition, mean-field theory does not allow one to take into account higher-order corrections to the stability condition. The latter are considered further in Appendix B.

V. SUPPRESSION OF OSTWALD RIPENING IN 2D

Since the balance condition (4.2) and the leading-order stability condition (4.13) are identical in form to those obtained previously using mean-field theory in 3D, we will focus on analyzing the suppression of Ostwald ripening for circular droplets. Analogous to Refs. [14,18], we analyze the dynamics in two separate regimes corresponding to the cases $\rho^* \ll \xi$ (small-droplet regime) and $\rho^* \gg \xi$ (large-droplet regime). Here the size of a droplet is in reference to the length constant ξ rather than the mean separation L.

A. Large-droplet regime

Suppose that $\rho^* \gg \xi$. Consider the asymptotic expansions

$$I_0(z) \sim \frac{e^z}{\sqrt{2\pi z}} \left[1 + \frac{1}{8z} + O(z^{-2}) \right],$$

$$I_0'(z) \sim \frac{e^z}{\sqrt{2\pi z}} \left[1 - \frac{3}{8z} + O(z^{-2}) \right], \tag{5.1}$$

and

$$K_0(z) \sim e^{-z} \sqrt{\frac{\pi}{2\pi z}} \left[1 - \frac{1}{8z} + O(z^{-2}) \right],$$

$$K_0'(z) \sim -e^{-z} \sqrt{\frac{\pi}{2\pi z}} \left[1 + \frac{3}{8z} + O(z^{-2}) \right]. \tag{5.2}$$

These imply that

$$\frac{I_0'(z)}{I_0(z)} = \frac{1 - 3/8z}{1 + 1/8z} + O(z^{-2}) \approx 1 - \frac{1}{2z} \tag{5.3}$$

and

$$-\frac{K_0'(z)}{K_0(z)} = \frac{1 + 3/8z}{1 - 1/8z} + O(z^{-2}) \approx 1 + \frac{1}{2z}. \tag{5.4}$$

Substituting these asymptotic expansions into Eq. (3.33), gives to leading order in ξ/ρ^*

$$J_-(\rho, \Theta) \approx \frac{D}{\xi} \left(\frac{\beta}{\alpha + \beta} \phi_b - \frac{\alpha \Theta}{\alpha + \beta} \right) \left(1 - \frac{\xi}{2\rho} \right), \tag{5.5a}$$

$$J_+(\rho, \Theta) \approx \frac{D}{\xi} \left\{ \frac{\alpha \Theta}{\alpha + \beta} - \frac{\beta}{\alpha + \beta} \phi_a \left(1 + \frac{1}{\rho} \right) \right\}$$

$$\times \left(1 + \frac{\xi}{2\rho} \right). \tag{5.5b}$$

1. Steady-state radius

Substituting Eqs. (5.5) into the balance condition (4.2) shows that to leading order in ξ/ρ^*,

$$\frac{\beta}{\alpha + \beta} \phi_b - \frac{\alpha \Theta^*}{\alpha + \beta} = \frac{\alpha \Theta^*}{\alpha + \beta} - \frac{\beta}{\alpha + \beta} \phi_a \left(1 + \frac{1}{\rho^*} \right)$$

Combining with Eq. (4.1) implies that

$$\phi_b - \Phi_b \approx \phi_\infty - \phi_a \left(1 + \frac{1}{\rho^*} \right), \tag{5.6}$$

where Φ_b is the mean concentration within each droplet,

$$\Phi_b = \frac{\alpha}{\alpha + \beta} (\Theta^* + \phi_b). \tag{5.7}$$

Next, imposing solute mass conservation gives

$$\pi \rho^{*2} N \Phi_b + (A - \pi \rho^{*2} N) \phi_\infty \approx A \phi_{tot}, \tag{5.8}$$

where $A = |\Omega|$ is the total area of the system and $\phi_{tot} = \alpha u_{tot}/(\alpha + \beta)$ is the original homogeneous concentration of P molecules. For simplicity, the concentration gradients near the interface have been neglected since the interfacial region is small compared to the size of the droplets ($\xi \ll \rho^*$). Rearranging Eq. (5.8),

$$\pi \rho^{*2} = \frac{A}{N} \frac{\phi_{tot} - \phi_\infty}{\Phi_b - \phi_\infty}.$$

Following along similar lines to Ref.[14], Eqs. (5.6) and (5.7) imply that

$$\pi \rho^{*2} \approx \frac{A}{N}\left[\frac{u_{\text{tot}} - \phi_a(1 + 1/\rho^*)}{\phi_b} - \frac{\beta}{2\alpha}\right], \qquad (5.9)$$

after using $\phi_b \gg \phi_a$. For the sake of illustration, suppose that $\rho^* \gg 1$. Taking $A/N^2 = L^2 = 1$, with L the average droplet separation, we then have

$$\pi \rho^{*2} = N\left(\frac{u_{\text{tot}} - \phi_a}{\phi_b} - \frac{\beta}{2\alpha}\right). \qquad (5.10)$$

Note that the radius ρ^* is an extensive variable, that is, it depends on the number of droplets N. Assuming that $N \gg 1$, then this condition will be satisfied if $\beta < \beta_u(\alpha)$ with

$$\beta_u(\alpha) = 2\alpha\left(\frac{u_{\text{tot}} - \phi_a}{\phi_b}\right). \qquad (5.11)$$

2. Stability of the multidroplet state

In order to determine the stability of the multidroplet solution, we have to calculate the various first-order derivatives in Eq. (4.13). From Eqs. (5.5),

$$\frac{\partial J_-}{\partial \rho} \approx \frac{D}{2\rho^2}\frac{\beta\phi_b - \alpha\Theta}{\alpha + \beta},$$

$$\frac{\partial J_+}{\partial \rho} \approx -\frac{D}{2\rho^2}\frac{\alpha\Theta - \beta\phi_a[1 + 1/\rho]}{\alpha + \beta} + \frac{D}{\xi}\frac{\beta\phi_a}{\rho^2(\alpha + \beta)},$$

$$\frac{\partial J_-}{\partial \Theta} \approx -\frac{\alpha D}{\xi(\alpha + \beta)}\left(1 - \frac{\xi}{2\rho}\right),$$

$$\frac{\partial J_+}{\partial \Theta} = \frac{\alpha D}{\xi(\alpha + \beta)}\left(1 + \frac{\xi}{2\rho}\right).$$

Substituting into Eq. (4.11) shows that

$$\delta J_i \sim \frac{\nu D}{\rho^{*3}}\left[\phi_a - \frac{\beta(\phi_b\xi - 2\phi_a)}{2\alpha}\right]\delta\rho_i, \qquad (5.12)$$

after using $\phi_b \gg \phi_a$ and $\xi \ll \rho^*$. We conclude that the droplets will be stable with respect to local perturbations provided that $\beta > \beta_l(\alpha)$ where

$$\beta_l(\alpha) = \frac{2\phi_a\alpha}{\phi_b\xi - 2\phi_a}. \qquad (5.13)$$

In summary, in the large-droplet regime, a stable multidroplet steady state with $\rho_i = \rho^*$ and $\Theta_i = \Theta^*$ exists for a range of values of the switching rate β and fixed α:

$$\beta_l(\alpha) < \beta < \beta_u(\alpha).$$

The upper and lower bounds β_u and β_l are almost identical to the 3D case [14]. However, there are $O(\nu)$ corrections to these bounds, see Appendix B.

B. Small-droplet regime

Now suppose that $\rho^* \ll \xi$ and consider the following small-z expansion of the modified Bessel function $I_0(z)$,

$$I_0(z) = 1 + \frac{z^2}{4} + \frac{1}{(2!)^2}\left(\frac{z^2}{4}\right)^2 + \cdots, \qquad (5.14)$$

we have

$$\frac{I_0'(z)}{I_0(z)} = \frac{z/2 + z^3/16 + \cdots}{1 + z^2/4} = \frac{z}{2} - \frac{z^3}{16} + O(z^5).$$

Hence, to leading order in ρ/ξ,

$$J_-(\rho, \Theta) \approx \frac{D}{2\xi^2}\left(\frac{\beta}{\alpha + \beta}\phi_b - \frac{\alpha\Theta}{\alpha + \beta}\right)\rho \approx \frac{\beta}{2}\phi_b\rho. \quad (5.15)$$

This flux is consistent with the fact that the number of droplet P molecules converted to S molecules per unit time is $p = \beta\pi\rho_i^2\phi_b$ and the S molecules rapidly diffuse out of the droplet to generate a flux $J \approx p/(2\pi\rho_i) = \beta\pi\rho_i\phi_b/2$. Similarly, using a small-z expansion of the modified Bessel function $K_0(z)$,

$$K_0(z) = -[\ln(z/2) + \gamma]I_0(z) + \frac{z^2}{2} + \frac{3}{2}\frac{z^4}{64} + \cdots, \quad (5.16)$$

where γ is the Euler constant, we find that

$$J_+(\rho, \Theta) \approx \frac{D}{\rho}\left\{\frac{\alpha\Theta}{\alpha + \beta} - \frac{\beta}{\alpha + \beta}\phi_a\left(1 + \frac{1}{\rho}\right)\right\}\frac{1}{|\ln(\rho/2\xi)|}. \qquad (5.17)$$

Substituting these asymptotic expansions into Eq. (4.2) and using Eq. (4.1), gives to leading order in ρ^*/ξ the balance condition

$$\frac{\beta}{2}\phi_b\rho^* = \frac{D}{\rho^*}\left\{\Delta - \frac{\phi_a}{\rho^*}\right\}\frac{1}{|\ln(\rho^*/2\xi)|}, \qquad (5.18)$$

where $\Delta = \phi_\infty - \phi_a$ is the supersaturation. Equation (5.18) is similar in form to the balance equation for small 3D droplets derived in Refs. [14,18] using mean-field theory. One major difference is the presence of the additional logarithmic factor $1/\ln(\rho^*/2\xi)$, which means that the existence of a multidroplet steady state now depends on ξ to leading order. The existence of steady-state multidroplet solutions can be investigated graphically as illustrated in Fig. 6. Here we plot the fluxes $J_\pm(\rho^*, \Theta^*)$ as functions of ρ^* with Θ^* given by Eq. (4.1). The latter holds in the case of a solution for which all droplets have the same radius. Points of intersection of the curves $J_\pm$ correspond to multidroplet solutions that are stationary with respect to droplet growth due to the fluxes balancing. It can be seen that for a range of supersaturations Δ and interfacial length constants ξ, there exists a pair of steady state radii $\rho_\pm^*$. However, these steady-state solutions disappear for sufficiently small Δ or large ξ.

We also see that the solution with radius ρ_+^* is stable, whereas the other solution with radius ρ_-^* is unstable. This is based on the observation that $J_+ > J_-$ for $\rho_* < \rho_+^*$ and $J_+ < J_-$ for $\rho_* > \rho_+^*$ so that a larger droplet has a net efflux, whereas a smaller droplet has a net influx. The opposite holds in a neighborhood of ρ_-^*. In other words, a multidroplet state is stable if

$$\frac{\partial J_+}{\partial \rho^*} < \frac{\partial J_-}{\partial \rho^*}. \qquad (5.19)$$

VI. DISCUSSION

In this paper we used asymptotic methods to investigate the suppression of Ostwald ripening in a model of active liquid-liquid phase separation, which was previously analyzed using
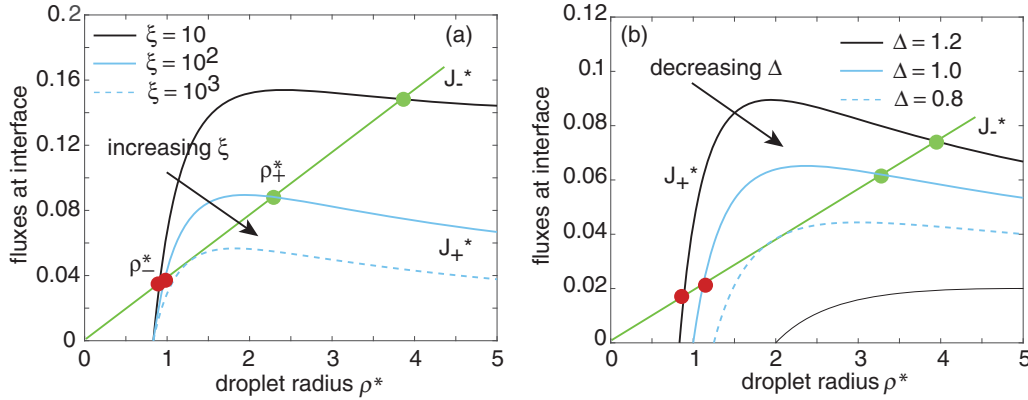
FIG. 6. Active suppression of Ostwald ripening in the small-droplet regime ($\xi/\rho^* \ll 1$). In a multidroplet state $(\rho_i, \Theta_i) = (\rho^*, \Theta^*)$, $i = 1, \ldots, N$, the net flux at a droplet interface is a combination of an influx $J_+^* = J_+(\rho^*)$ and an efflux $J_-^* = J_-(\rho^*)$ where we have set $\Theta^* = u_\infty - \phi_a(1 + 1/\rho^*)$. A solution is a steady state with respect to droplet growth provided that the fluxes are balanced. For fixed supersaturation $\Delta = \phi_\infty - \phi_a$ and interfacial length constant ξ, steady states correspond to points of intersection of the curves $J_+(\rho^*)$ and $J_-(\rho^*)$. (a) Plots of $J_+(\rho^*)$ as a function of ρ^* for various ξ values and fixed supersaturation $\Delta = 1.2$ (b) Plots of $J_+(\rho^*)$ as a function of ρ^* for various Δ values and fixed $\xi = 100$. For a range of values of Δ and ξ, there exist two steady-state radii $\rho_\pm^*$ for which the fluxes cancel. These steady states disappear below a critical supersaturation or above a critical interfacial length constant ξ. Other parameters are $D = 1$ and $\phi_a = 1$.

mean-field theory [14,18,19]. Two limitations of the latter approach are that (i) it breaks down in the case of 2D droplets due to logarithmic singularities, and (ii) it cannot take into account finite size effects. The two main assumptions of our analysis were that the droplets are well separated and that they are relatively small. In particular, taking the mean separation to be L, we introduced the small parameter $\epsilon = \ell_c/L$, where ℓ_c is the capillary length associated with the Gibbs-Thomson law, and took the droplet radii to have the scaling $R_i/L = \epsilon \rho_i$. It immediately follows that one limitation of our approach is that it cannot deal with dense droplet condensates or droplets whose size are comparable to the size of the domain. The main results and implications of our analysis are as follows.

(i) The existence and stability of multiple droplet states in active liquid-liquid phase separation (active suppression of Ostwald ripening) can be formulated as a diffusion problem in a domain with small exclusions or holes. This type of problem requires dealing with strongly localized perturbations, that is, perturbations of large magnitude but small spatial extent [31,34,35]. Such singular perturbations have received considerable attention in recent years within the context of the so-called narrow escape problem, see the recent reviews [39,40]. That is, molecules inside the cell are often confined to a domain with small exits on the boundary of the domain or traps within the interior of the domain. Examples include the transport of newly transcribed mRNA from the nucleus to the cytoplasm via nuclear pores, the confinement of neurotransmitter receptors within a synapse of a neuron, and the confinement of calcium and other signaling molecules within subcellular compartments such as dendritic spines. In the case of narrow escape problems, one is typically interested in solving a first passage time problem in which the boundary of each exclusion is taken to be absorbing. This differs significantly from the problem considered in this paper, where one also has to consider diffusion within the interior of each exclusion or droplet, and impose (possibly discontinuous) boundary conditions across each droplet interface. Moreover,

the diffusing species are in quasisteady state due to the slow growth or shrinkage of the droplets.

(ii) In determining the stability of a multidroplet state, it is necessary to consider fluctuations in each droplet radius ρ_i and the corresponding concentration Θ_i of the non-phase-separating (S) solute at the interface. The latter is determined by imposing continuity of the S flux. One consequence of this is that, away from the steady state, there is an additional contribution to the influx of the phase-separating (P) solute at the interface, which is given by the spatial gradient of the total solution concentration. Thus, within a boundary layer around each droplet, one cannot take this gradient to be zero.

(iii) One major difference between the asymptotic analysis of 2D and 3D droplets is that the former involves an asymptotic expansion in $\nu = -1/\ln \epsilon$, whereas the latter involves an asymptotic expansion in ϵ. Since $\nu \to 0$ more slowly than $\epsilon \to 0$, one can achieve greater accuracy for fixed ϵ in the 3D case. Following [31], it is possible to sum all logarithmic terms, but this is less useful for practical calculations except in the simplest geometric configurations.

(iv) Keeping only leading-order terms in the asymptotic expansions, it is possible to derive explicit conditions for the existence and stability of a multidroplet state, which recover the results of mean-field theory for 3D droplets. A number of differences emerge, however, when analyzing the corresponding leading-order conditions in 2D. First, fluctuations about the multidroplet steady state are $O(\nu)$ rather than $O(1)$. Second, in the small-droplet regime ($\rho^* \ll \xi$) the in-flux has an additional logarithmic factor of the form $-1/\ln(\rho^*/\xi)$, where ρ^* is the steady-state droplet radius and ξ is the width of each interfacial region. This means that the existence of the multidroplet state has a leading-order dependence on ξ as well as the supersaturation Δ. Higher-order terms in the asymptotic expansions take into account finite-size effects associated with the boundary of the domain and the positions of the droplets. These modify the stability condition for the multidroplet solution, but not the existence condition.

(v) Although we applied the theory of strongly localized perturbations to a specific model of active liquid-liquid phase separation [14,18,19], the underlying asymptotic methods have a wide range of applicability, as has been demonstrated in other problem domains [31–40]. Possible generalizations include different mechanisms for active phase separation such as autocatalysis [19,22], heterogeneous media including droplet ripening in protein concentration gradients [21], different interfacial boundary conditions, and eigenvalue problems associated with the approach to steady state. In the case of the regulation of droplet ripening by protein concentration gradients, one finds that perturbations of spherical droplets are no longer radially symmetric, and this induces a slow drift of 3D droplets down the concentration gradient [19,21]. This is analogous to the observation of droplet segregation during asymmetric cell division of *C. elegans* zygotes. It should be possible to investigate analogous drift phenomena in the case of 2D droplets by adapting the asymptotic methods of this paper.

APPENDIX A: NEUMANN GREEN'S FUNCTIONS IN SIMPLE GEOMETRIES.

(a) *The disk.* Let $\Omega \subset \mathbb{R}^2$ be the unit circle centered at the origin. The 2D Neumann Green's function is given by [24]:

$$G^{(2)}(\mathbf{x}, \boldsymbol{\xi}) = \frac{1}{2\pi}\left[-\ln(|\mathbf{x} - \boldsymbol{\xi}|) - \ln\left(\left|\mathbf{x}|\boldsymbol{\xi}| - \frac{\boldsymbol{\xi}}{|\boldsymbol{\xi}|}\right|\right)\right. \\ \left. + \frac{1}{2}(|\mathbf{x}|^2 + |\boldsymbol{\xi}|^2) - \frac{3}{4}\right], \quad \text{(A1)}$$

with the regular part obtained by dropping the first logarithmic term.

(b) *The sphere.* Let $\Omega \subset \mathbb{R}^3$ be the sphere of radius a centered about the origin. The 3D Neumann Green's function takes the form [41]

$$G^{(3)}(\mathbf{x}, \boldsymbol{\xi}) = \frac{1}{4\pi|\mathbf{x} - \boldsymbol{\xi}|} + \frac{a}{4\pi|\mathbf{x}|r'} \\ + \frac{1}{4\pi a}\ln\left(\frac{2a^2}{a^2 - |\mathbf{x}||\boldsymbol{\xi}|\cos\theta + |\mathbf{x}|r'}\right) \\ + \frac{1}{6|\Omega|}(|\mathbf{x}|^2 + |\boldsymbol{\xi}|^2) + B, \quad \text{(A2)}$$

where the constant B is chosen so that $\int_\Omega G^{(3)}(\mathbf{x}, \boldsymbol{\xi})d\mathbf{x} = 0$, and

$$\cos\theta = \frac{\mathbf{x} \cdot \boldsymbol{\xi}}{|\mathbf{x}||\boldsymbol{\xi}|}, \quad \mathbf{x}' = \frac{a^2\mathbf{x}}{|\mathbf{x}|^2}, \quad r' = |\mathbf{x}' - \boldsymbol{\xi}|.$$

It can be shown that B is independent of $\boldsymbol{\xi}$.

(c) *Rectangular domain.* Let $\Omega \subset \mathbb{R}^2$ be a rectangular domain $[0, L_1] \times [0, L_2]$. The 2D Neumann Green's function has the logarithmic expansion [34]

$$G^{(2)}(\mathbf{r}, \mathbf{r}') = \frac{1}{L_1}H_0(y, y') - \frac{1}{2\pi}\sum_{j=0}^{\infty}\sum_{n=\pm}\sum_{m=\pm}(\ln|1 - \tau^j z_n \zeta_m| \\ + \ln|1 - \tau^j z_n \varsigma_m|), \quad \text{(A3)}$$

where

$$\tau = e^{-2\pi L_2/L_1}, \qquad z_\pm = e^{i\pi(x\pm x')/L_1},$$

$$\zeta_\pm = e^{-\pi|y\pm y'|/L_1}, \quad \varsigma_\pm = e^{-\pi(2L_2 - |y\pm y'|)/L_1},$$

and

$$H_0(y, y') = \frac{L_2}{3} + \frac{1}{2L_2}(y^2 + y'^2) - \max\{y, y'\}, \quad \text{(A4)}$$

Assuming that $\tau \ll 1$, we have the approximation

$$G^{(2)}(\mathbf{r}, \mathbf{r}') = \frac{1}{L_1}H_0(y, y') - \frac{1}{2\pi}\sum_{n=\pm}\sum_{m=\pm}(\ln|1 - z_n \zeta_m| \\ + \ln|1 - z_n \varsigma_m|) + \mathcal{O}(\tau). \quad \text{(A5)}$$

The only singularity exhibited by Eq. (A3) occurs when $\mathbf{r} \to \mathbf{r}'$, $\mathbf{r}' \notin \partial\Omega$, in which case $z_- = \zeta_- = 1$ and the term $\ln|1 - z_-\zeta_-|$ diverges. Writing

$$\ln|1 - z_-\zeta_-| = \ln|\mathbf{r} - \mathbf{r}'| + \ln\frac{|1 - z_-\zeta_-|}{|\mathbf{r} - \mathbf{r}'|}, \quad \text{(A6)}$$

where the first term on the right-hand side is singular and the second is regular, we find that

$$G^{(2)}(\mathbf{r}, \mathbf{r}') = -\frac{1}{2\pi}\ln|\mathbf{r} - \mathbf{r}'| + R(\mathbf{r}, \mathbf{r}'), \quad \text{(A7)}$$

where R is the regular part of the Green's function given by

$$R(\mathbf{r}, \mathbf{r}') = -\frac{1}{L_1}H_0(y, y') + \frac{1}{2\pi}\ln\frac{|1 - z_-\zeta_-||1 - z_-\zeta_+|}{|\mathbf{r} - \mathbf{r}'|}$$

$$\frac{1}{2\pi}\ln|1 - z_-\varsigma_-||1 - z_-\varsigma_+|$$

$$\frac{1}{2\pi}\ln|1 - z_+\varsigma_-||1 - z_+\varsigma_+|$$

$$\frac{1}{2\pi}\ln|1 - z_+\zeta_-||1 - z_+\zeta_+| + O(\tau). \quad \text{(A8)}$$

APPENDIX B: HIGHER-ORDER CORRECTIONS TO MULTIDROPLET STABILITY

In Sec. IV, we derived the $O(1)$ stability condition (4.13) by Taylor expanding the fluxes j_i to leading order in ν (2D) or ϵ (3D). Here we indicate how to extend the analysis to include higher-order terms.

1. 2D droplets

In order to determine the matrices **P** and **Q** of Eq. (4.5), we rewrite Eq. (3.19) as

$$\sum_{i=1}^{N}[\delta_{i,j} + \nu M_{ji}]B_i(\boldsymbol{\rho}, \boldsymbol{\Theta}) = u_\infty - \phi_a\left(1 + \frac{1}{\rho_j}\right) - \Theta_j \quad \text{(B1)}$$

Differentiating both sides of Eq. (B1) with respect to ρ_k and noting from Eq. (2.22) that

$$\frac{\partial M_{jj}}{\partial \rho_k} = -\frac{\delta_{j,k}}{\rho_j}, \quad \frac{\partial M_{ji}}{\partial \rho_k} = 0 \quad \text{for } i \neq j,$$

we have

$$\frac{\partial B_j}{\partial \rho_k} + \nu \sum_{i=1}^{N} M_{ji}\frac{\partial B_i}{\partial \rho_k} - \frac{\nu}{\rho_j}B_j\delta_{j,k} = \frac{\phi_a}{\rho_j^2}\delta_{j,k}.$$

Rearranging this equations yields

$$\frac{\partial B_i}{\partial \rho_k} = [\mathbf{I} + \nu\mathbf{M}]_{ik}^{-1}\left[\frac{\nu}{\rho_i}B_i + \frac{\phi_a}{\rho_i^2}\right]. \tag{B2}$$

Similarly, differentiating both sides of Eq. (B1) with respect to Θ_k and noting from Eq. (2.22) that

$$\frac{\partial M_{ij}}{\partial \rho_k} = 0 \quad \text{for all } i, j = 1, \dots, N,$$

we have

$$\frac{\partial B_j}{\partial \Theta_k} + \nu\sum_{i=1}^{N} M_{ji}\frac{\partial B_i}{\partial \Theta_k} = -\delta_{j,k}.$$

and hence

$$\frac{\partial B_i}{\partial \Theta_k} = -[\mathbf{I} + \nu\mathbf{M}]_{ik}^{-1}. \tag{B3}$$

It then follows from Eqs. (3.33d) and (4.5c) that

$$P_{il} = \frac{\alpha}{\alpha + \beta}\frac{\nu D\phi_a}{\rho^{*3}}[\mathbf{I} + \nu\mathbf{M}(\rho^*)]_{il}^{-1}, \tag{B4a}$$

$$Q_{il} = -\frac{\alpha}{\alpha + \beta}\frac{\nu D}{\rho^*}[\mathbf{I} + \nu\mathbf{M}(\rho^*)]_{il}^{-1}, \tag{B4b}$$

where

$$M_{ij}(\rho^*) = [2\pi R^{(2)}(\mathbf{x}_i, \mathbf{x}_i) - \ln\rho^*]\delta_{i,j} \\ + 2\pi G^{(2)}(\mathbf{x}_i, \mathbf{x}_j)(1 - \delta_{i,j}).$$

We have used the identity $B_i(\boldsymbol{\rho}^*, \boldsymbol{\Theta}^*) = 0$. Equations (4.6), (4.7), (B4a), and (B4b) provide a nonperturbative approximation to the effects of fluctuations on the multidroplet state, in which all logarithmic terms have been summed. Clearly Eqs. (4.10) are recovered on dropping $O(\nu^2)$ terms. Here we determine the $O(\nu^2)$ corrections to the stability condition (4.13). Using

$$[\mathbf{I} + \nu\mathbf{M}]^{-1} = \mathbf{I} - \nu\mathbf{M} + O(\nu^2),$$

we have

$$\left[\mathcal{P}\mathbf{I} - \frac{\beta}{\alpha}\mathbf{P}\right]_{lk} \approx \left\{\frac{\partial J_+}{\partial \rho^*} - \frac{\partial J_-}{\partial \rho^*} - \frac{\beta}{\alpha + \beta}\frac{\nu D\phi_a}{\rho^{*3}}\right\}\delta_{l,k} \\ + \frac{\beta}{\alpha + \beta}\frac{\nu^2 D\phi_a}{\rho^{*3}}M_{lk}(\rho^*) + O(\nu^3),$$

and

$$\left[\mathcal{Q}\mathbf{I} - \frac{\beta}{\alpha}\mathbf{Q}\right]_{il} \approx \frac{1}{\gamma_2}\delta_{i,l} - \frac{\beta}{\alpha + \beta}\frac{\nu^2 D}{\rho^*}M_{il}(\rho^*) + O(\nu^3),$$

$$\gamma_2 = \frac{\Gamma_2}{\nu D} = \left[\frac{\partial J_+}{\partial \Theta^*} - \frac{\partial J_-}{\partial \Theta^*} + \frac{\beta}{\alpha + \beta}\frac{\nu D}{\rho^*}\right]^{-1}.$$

Equation (4.7) thus becomes

$$\delta\Theta_i = -\gamma_2\left\{\frac{\partial J_+}{\partial \rho^*} - \frac{\partial J_-}{\partial \rho^*} - \frac{\beta}{\alpha + \beta}\frac{\nu D\phi_a}{\rho^{*3}}\right\}\delta\rho_i \\ - \frac{\beta}{\alpha + \beta}\frac{\nu^2 D\gamma_2}{\rho^*}\left[\frac{\phi_a}{\rho^{*2}} + \gamma_2\left(\frac{\partial J_+}{\partial \rho^*} - \frac{\partial J_-}{\partial \rho^*}\right)\right] \\ \times \sum_{k=1}^{N} M_{ik}(\rho^*)\delta\rho_k + O(\nu^3). \tag{B5}$$

Finally, substituting into Eq. (4.6),

$$\delta J_i \approx \frac{\nu D\gamma_2}{\rho^*}\left\{\left[\frac{\partial J_+}{\partial \rho^*} - \frac{\partial J_-}{\partial \rho^*}\right] + \frac{\phi_a}{\rho^{*2}}\left[\frac{\partial J_+}{\partial \Theta^*} - \frac{\partial J_-}{\partial \Theta^*}\right]\right\} \\ \times \left[\delta\rho_i - \nu\gamma_2\sum_{k=1}^{N} M_{ik}(\rho^*)\delta\rho_k\right] + O(\nu^3) \tag{B6}$$

Hence, the stability condition (4.13) will still hold provided that

$$\nu\lambda_{\max} < \frac{\partial J_+}{\partial \Theta^*} - \frac{\partial J_-}{\partial \Theta^*}, \tag{B7}$$

where $\lambda_{\max}$ is the largest positive eigenvalue of the matrix $\mathbf{M}$.

Consider as an example a pair of droplets in the unit circle, whose Neumann Green's function is given by Eq. (A1). Taking both droplet centers to be on the x axis, $\mathbf{x}_j = (x_j, 0)$, $j = 1, 2$, it follows that

$$G^{(2)}(\mathbf{x}_1, \mathbf{x}_2) = \frac{1}{2\pi}\left[-\ln(|x_1 - x_2|) - \ln(|x_1 x_2 - 1|) \right. \\ \left. + \frac{1}{2}(x_1^2 + x_2^2) - \frac{3}{4}\right] = G(\mathbf{x}_2, \mathbf{x}_1), \tag{B8}$$

and

$$R^{(2)}(\mathbf{x}_j, \mathbf{x}_j) = \frac{1}{2\pi}\left[-\ln\left(|x_j^2 - 1|\right) + x_j^2 - \frac{3}{4}\right] \tag{B9}$$

for $j = 1, 2$. The matrix $\mathbf{M}(\rho^*)$ is then

$$\mathbf{M}(\rho^*) = \begin{pmatrix} 2\pi R_{11} - \ln\rho^* & 2\pi G_{12} \\ 2\pi G_{12} & 2\pi R_{22} - \ln\rho^* \end{pmatrix}, \tag{B10}$$

where we have set $R_{jj} = R^{(2)}(\mathbf{x}_j, \mathbf{x}_j)$ and $G_{12} = G^{(2)}(\mathbf{x}_1, \mathbf{x}_2)$. The eigenvalues of $\mathbf{M}$ are thus

$$\lambda_\pm = \pi[R_{11} + R_{22}] - \ln(\rho^*) \pm \pi\sqrt{(R_{11} - R_{22})^2 + G_{12}^2}. \tag{B11}$$

2. Three-dimensional droplets

One can also derive higher-order corrections to the stability condition for 3D droplets by carrying out a perturbation expansion in ϵ. We briefly highlight the leading-order correction. From Eqs. (3.24) and (3.34) and

$$j_i(\boldsymbol{\rho}, \boldsymbol{\Theta}) = \frac{\alpha}{\alpha + \beta}\frac{D}{\rho_i}\sum_{j=1}^{N}\{[1 - 4\pi\epsilon R^{(3)}(\mathbf{x}_i, \mathbf{x}_i)]\delta_{i,j} \\ - 4\pi\epsilon G^{(3)}(\mathbf{x}_i, \mathbf{x}_j)(1 - \delta_{i,j})\} \\ \times \left[u_\infty - \Theta_j - \phi_a\left(1 + \frac{1}{\rho_j}\right)\right] + O(\epsilon^2). \tag{B12}$$

Hence,

$$P_{il} = \frac{\alpha}{\alpha + \beta} \frac{D\phi_a}{\rho^{*3}} \{[1 - 4\pi\epsilon R^{(3)}(\mathbf{x}_i, \mathbf{x}_i)]\delta_{i,l} - 4\pi\epsilon G^{(3)}(\mathbf{x}_i, \mathbf{x}_l)(1 - \delta_{i,l})\}, \tag{B13a}$$

$$Q_{il} = -\frac{\alpha}{\alpha + \beta} \frac{D}{\rho^*} \{[1 - 4\pi\epsilon R^{(3)}(\mathbf{x}_i, \mathbf{x}_i)]\delta_{i,l} - 4\pi\epsilon G^{(3)}(\mathbf{x}_i, \mathbf{x}_l)(1 - \delta_{i,l})\}. \tag{B13b}$$

It follows that

$$\left[\mathcal{P}\mathbf{I} - \frac{\beta}{\alpha}\mathbf{P}\right]_{lk} \approx \left\{\frac{\partial J_+}{\partial \rho^*} - \frac{\partial J_-}{\partial \rho^*} - \frac{\beta}{\alpha + \beta}\frac{D\phi_a}{\rho^{*3}}\right\}\delta_{l,k} + \epsilon\frac{\beta}{\alpha + \beta}\frac{D\phi_a}{\rho^{*3}}\mathcal{G}_{lk} + O(\epsilon^2)$$

and

$$\left[\mathcal{Q}\mathbf{I} - \frac{\beta}{\alpha}\mathbf{Q}\right]_{il} \approx \frac{1}{\gamma_3}\delta_{i,l} - \epsilon\frac{\beta}{\alpha + \beta}\frac{D}{\rho^*}\mathcal{G}_{il} + O(\epsilon^2),$$

with

$$\mathcal{G}_{ij} = 4\pi R^{(3)}(\mathbf{x}_i, \mathbf{x}_i)\delta_{i,j} + 4\pi G^{(3)}(\mathbf{x}_i, \mathbf{x}_j)(1 - \delta_{i,j}), \quad \gamma_3 = \left[\frac{\partial J_+}{\partial \Theta^*} - \frac{\partial J_-}{\partial \Theta^*} + \frac{\beta}{\alpha + \beta}\frac{D}{\rho^*}\right]^{-1}.$$

Equation (4.7) thus becomes

$$\delta\Theta_i = -\gamma_3\left\{\frac{\partial J_+}{\partial \rho^*} - \frac{\partial J_-}{\partial \rho^*} - \frac{\beta}{\alpha + \beta}\frac{D\phi_a}{\rho^{*3}}\right\}\delta\rho_i - \epsilon\frac{\beta}{\alpha + \beta}\frac{D\gamma_3}{\rho^*}\left[\frac{\phi_a}{\rho^{*2}} + \gamma_3\left(\frac{\partial J_+}{\partial \rho^*} - \frac{\partial J_-}{\partial \rho^*}\right)\right]\sum_{k=1}^N \mathcal{G}_{ik}\delta\rho_k + O(\epsilon^2). \tag{B14}$$

Substituting into Eq. (4.6),

$$\delta J_i \approx \frac{D\gamma_3}{\rho^*}\left(\left\{\left[\frac{\partial J_+}{\partial \rho^*} - \frac{\partial J_-}{\partial \rho^*}\right] + \frac{\phi_a}{\rho^{*2}}\left[\frac{\partial J_+}{\partial \Theta^*} - \frac{\partial J_-}{\partial \Theta^*}\right]\right\}\delta\rho_i - \epsilon\left[\frac{\phi_a}{\rho^{*2}} + \gamma_3\left(\frac{\partial J_+}{\partial \rho^*} - \frac{\partial J_-}{\partial \rho^*}\right)\right]\sum_{k=1}^N \mathcal{G}_{ik}\delta\rho_k\right) + O(\epsilon^2). \tag{B15}$$

[1] C. P. Brangwynne *et al.*, Germline P granules are liquid droplets that localize by controlled dissolution/condensation, Science **324**, 1729 (2009).

[2] C. P. Brangwynne, T. J. Mitchison, and A. A. Hyman, Active liquid-like behavior of nucleoli determines their size and shape in Xenopus laevis oocytes, Proc. Natl. Acad. Sci. USA **108**, 4334 (2011).

[3] S. Elbaum-Garfinkle *et al.*, The disordered P granule protein LAF-1 drives phase separation into droplets with tunable viscosity and dynamics, Proc. Natl. Acad. Sci. USA **112**, 7189 (2015).

[4] A. A. Hyman, C. A. Weber, and F. Julicher, Liquid-liquid phase separation in biology, Annu. Rev. Cell Dev. Biol. **30**, 39 (2014).

[5] C. P. Brangwynne, P. Tompa, and R. V. Pappu, Polymer physics of intracellular phase transitions, Nat. Phys. **11**, 899 (2015).

[6] S. F. Banani, H. O. Lee, A. A. Hyman, and M. K. Rosen, Biomolecular condensates: Organizers of cellular biochemistry, Nat. Rev. Mol. Cell Biol. **18**, 285 (2017).

[7] J. Berry, C. Brangwynne, and H. P. Haataja, Physical principles of intracellular organization via active and passive phase transitions, Rep. Prog. Phys. **81**, 046601 (2018).

[8] H. Falahati and A. Haji-Akbari, Thermodynamically driven assemblies and liquid-liquid phase separations in biology, Soft Matter **15**, 1135 (2019).

[9] P. Li *et al.*, Phase transitions in the assembly of multivalent signaling proteins, Nature **483**, 336 (2012).

[10] S. Banjade and M. K. Rosen, Phase transitions of multivalent proteins can promote clustering of membrane receptors, eLife **3**, e04123 (2014).

[11] I. M. Lifshitz and V. V. Slyozov, The kinetics of precipitation from supersaturated solid solutions, J. Phys. Chem. Solids. **19**, 35 (1961).

[12] C. Wagner, Theorie der Alterung von Niederschlägen durch Umlösen, Z. Elektrochem. **65**, 581 (1961).

[13] M. Doi, *Soft Matter Physics* (Oxford University Press, Oxford, 2013).

[14] C. F. Lee and J. D. Wurtz, Novel physics arising from phase transitions in biology, J. Phys. D **52**, 023001 (2019).

[15] S. Jain *et al.*, ATPase-modulated stress granules contain a diverse proteome and substructure, Cell **164**, 487 (2016).

[16] M. Feric and C. P. Brangwynne, A nuclear F-actin scaffold stabilizes ribonucleoprotein droplets against gravity in large cells, Nat. Cell Biol. **15**, 1253 (2013).

[17] D. Zwicker, A. A. Hyman, and F. Jülicher, Suppression of Ostwald ripening in active emulsions, Phys. Rev. E **92**, 012317 (2015).

[18] J. D. Wurtz and C. F. Lee, Chemical-Reaction-Controlled Phase Separated Drops: Formation, Size Selection and Coarsening, Phys. Rev. Lett. **120**, 078102 (2018).

[19] C. A. Weber, D. Zwicker, F. Jülicher, and C. F. Lee, Physics of active emulsions. Rep. Prog. Phys. **82**, 064601 (2019).

[20] C. F. Lee, C. P. Brangwynne, J. Gharakhani, A. A. Hyman, and F. Julicher, Spatial Organization of the Cell Cytoplasm

by Position-Dependent Phase Separation, Phys. Rev. Lett. **111**, 088101 (2013).

[21] C. A. Weber, C. F. Lee, and F. Jülicher, F. Droplet ripening in concentration gradients, New J. Phys. **19**, 053021 (2017).

[22] D. Zwicker, M. Decker, S. Jaensch, A. A. Hyman, and F. Jülicher, Centrosomes are autocatalytic drops of pericentriolar material organized by centrioles, Proc. Natl. Acad. Sci. USA **111**, E2636 (2014).

[23] N. D. Alikakos, G. Fusco, and G. Karali, Ostwald ripening in two dimensions—The rigorous derivation of the equations from the Mullins-Sekerka dynamics, J. Diff. Eqs. **205**, 1 (2004).

[24] E. Kavanagh, *Interface Motion in the Ostwald Ripening and Chemotaxis Systems*. Master's thesis, University of British Columbia (2014).

[25] S. Ramaswamy and M. Rao, The physics of active membranes, C. R. Acad. Sci. Paris **2**, 817 (2001).

[26] H. Y. Chen, Internal States of Active Inclusions and the Dynamics of an Active Membrane, Phys. Rev. Lett. **92**, 168101 (2004).

[27] A. Veksler and N. S. Gov, Phase transitions of the coupled membrane-cytoskeleton modify cellular shape, Biophys. J. **93**, 3798 (2007).

[28] M. M. Kozlov, F. Campelo, N. Liska, L. V. Chernomordik, S. J. Marrink, and H. T. McMahon, Mechanisms shaping cell membranes, Curr. Opin. Cell. Biol. **29**, 53 (2014).

[29] N. S. Gov, Guided by curvature: Shaping cells by coupling curved membrane proteins and cytoskeletal forces, Roy. Soc. Phil Trans. B **373**, 20170115 (2018).

[30] M. M. Fryd and T. G. Mason, Advanced nanoemulsions, Annu. Rev. Phys. Chem. **63**, 493 (2012).

[31] M. J. Ward, W. D. Henshaw, and J. B. Keller, Summing logarithmic expansions for singularly perturbed eigenvalue problems, SIAM J. Appl. Math. **53**, 799 (1993).

[32] P. C. Bressloff, B. A. Earnshaw, and M. J. Ward, Diffusion of protein receptors on a cylindrical dendritic membrane with partially absorbing traps, SIAM J. Appl. Math. **68**, 1223 (2008).

[33] D. Coombs, R. Straube, and M. J. Ward, Diffusion on a sphere with localized traps: Mean first passage time, eigenvalue asymptotics, and Fekete points, SIAM J. Appl. Math **70**, 302 (2009).

[34] S. Pillay, M. J. Ward, A. Peirce, and T. Kolokolnikov, An asymptotic analysis of the mean first passage time for narrow escape problems: Part I: Two-dimensional domains, SIAM Multiscale Model. Sim. **8**, 803 (2010).

[35] A. F. Cheviakov, M. J. Ward, and R. Straube, An asymptotic analysis of the mean first passage time for narrow escape problems: Part II: The sphere, SIAM J. Multiscal Model. Sim. **8**, 836 (2010).

[36] P. C. Bressloff and S. D. Lawley, Escape from subcellular domains with randomly switching boundaries, Multiscale Model. Simul. **13**, 1420 (2015).

[37] R. Straube, M. J. Ward, and M. Falcke, Reaction rate of small diffusing molecules on a cylindrical membrane, J. Stat. Phys. **129**, 377 (2007).

[38] P. C. Bressloff and S. D. Lawley, Stochastically-gated diffusion-limited reactions for a small target in a bounded domain, Phys. Rev. E **92**, 062117 (2015).

[39] D. Holcman and Z. Schuss, Control of flux by narrow passages and hidden targets in cellular biology, Rep. Prog. Phys. **76**, 074601 (2013).

[40] D. Holcman and Z. Schuss, The narrow escape problem, SIAM Rev. **56**, 213 (2014).

[41] A. F. Cheviakov and M. J. Ward, Optomizing the principal eigenvalue of the Laplacian in a sphere with interior traps, Math. Comp. Model. **53**, 1394 (2011).